

## Local-field study of phase conjugation in metallic quantum wells with probe fields of both propagating and evanescent character

Torsten Andersen\* and Ole Keller

*Institute of Physics, Aalborg University, Pontoppidanstræde 103, DK-9220 Aalborg Øst, Denmark*

(Received 19 April 1999; revised manuscript received 3 August 1999)

The phase conjugated response from nonmagnetic multilevel metallic quantum wells is analyzed and an essentially complete analytical solution is presented and discussed. The description is based on a semiclassical local-field theory for degenerate four-wave mixing in mesoscopic interaction volumes of condensed media developed by the present authors [T. Andersen and O. Keller, *Phys. Scr.* **58**, 132 (1998)]. The analytical solution is supplemented by a numerical analysis of the phase conjugated response from a two-level quantum well in the case where one level is below the Fermi level and the other level is above. This is the simplest configuration of a quantum-well phase conjugator in which the light-matter interaction can be tuned to resonance. The phase conjugated response is examined in the case where all the scattering takes place in one plane, and linearly polarized light is used in the mixing. In the numerical work we study a two-monolayer thick copper quantum well using the infinite barrier model potential. Our results show that the phase conjugated response from such a quantum-well system is highly dependent on the spatial dispersion of the matter response. The resonances showing up in the numerical results are analytically identified from the expressions for the linear and nonlinear response tensors. In addition to the general discussion of the phase conjugated response with varying frequency and parallel component of the wave vector, we present the phase conjugated response in the special case where the light is in resonance with the interband transition.

[S0163-1829(99)03448-7]

### I. INTRODUCTION

Since the birth of nonlinear optics<sup>1</sup> as a discipline in physics nonlinear optical processes have been of great interest to scientists, for instance to help describe surfaces and interfaces of condensed matter.<sup>2-4</sup> Studies of surfaces and interfaces of condensed media belong to the regime of mesoscopic physics, where also quantum wells, wires, and dots can be found.<sup>5,6</sup> Among the many nonlinear optical phenomena that has been studied in the regime of mesoscopic physics are (i) second harmonic generation from magnetic<sup>7-10</sup> as well as nonmagnetic<sup>11-19</sup> systems, (ii) sum and difference frequency generation,<sup>16,20</sup> of which one of the most prominent applications today is Sisyphus cooling of atoms,<sup>21-23</sup> (iii) photon drag,<sup>24-27</sup> (iv) dc-electric-field induced second harmonic generation,<sup>28,29</sup> (v) the second-order Kerr effect,<sup>9,30-34</sup> (vi) electronic and vibrational surface Raman scattering,<sup>35-37</sup> (vii) two-photon photoemission,<sup>38-44</sup> (viii) generation of higher harmonics,<sup>45,46</sup> (ix) the second-order Lorenz-Mie scattering,<sup>47</sup> and (x) degenerate four-wave mixing.<sup>48-52</sup>

In the present paper we study phase conjugation by degenerate four-wave mixing in a quantum-well structure, where both interband and intraband transitions are allowed. Phase conjugation is a nonlinear process where the response field is counterpropagating to an incoming probe field. The usual descriptions (see Refs. 53-57, and references therein) of degenerate four-wave mixing (DFWM) are based on the assumption that the field amplitudes are slowly varying on the optical wavelength scale [slowly varying envelope (SVE) approximation], and thus also on the electric dipole (ED) approximation. We have previously presented the reasons (in Refs. 58 and 49) why these approximations are invalid when

considering optical interactions with matter of mesoscopic size, especially when evanescent components of the optical field are present. Four-wave mixing in media with two-dimensional translational invariance has so far been studied by other authors in the context of phase conjugation of electromagnetic surface waves,<sup>59-61</sup> and of a bulk wave by surface waves.<sup>62-70</sup> In these investigations macroscopic electrodynamic approaches were used. In order to go beyond the SVE and ED approximations a nonlocal microscopic theoretical model for optical phase conjugation by DFWM has been constructed (see Ref. 58) for nonmagnetic media. In addition to avoiding the SVE and ED approximations, other usually made approximations when considering optical phase conjugation are avoided in our model, namely, (i) the paraxial approximation, (ii) the assumption of a lossless medium, (iii) the assumption of a weak probe field, and (iv) the requirement of phase matching between the interacting fields.

In a two-dimensional translationally invariant system the change in energy of an electron due to an electric field can either involve a change of momentum along the translationally invariant plane (intraband transition), a change of energy eigenstate perpendicular to the translationally invariant plane (interband transition), or both. The change of momentum along the translationally invariant plane occurs as an addition of the momentum parallel to the plane of the interacting field component (denoted by  $\mathbf{q}_{\parallel}$ ) to (or subtraction from) the momentum of the electron parallel to the surface (denoted  $\kappa_{\parallel}$ ). It is thus convenient to divide the photon momentum  $\mathbf{q}$  into its components parallel and perpendicular to that plane, i.e.,  $\mathbf{q} = (\mathbf{q}_{\parallel}, q_{\perp})$ . Then the vacuum dispersion relation  $\mathbf{q} \cdot \mathbf{q} = q^2 = \omega^2/c_0^2$  provides us with an extra degree of freedom, since  $q_{\parallel} = |\mathbf{q}_{\parallel}|$  can be larger than  $\omega/c_0$ . Using the vacuum disper-

sion relation we find that  $q_{\perp}$  becomes imaginary in that case. In the following, propagating field components thus shall refer to the case where  $q_{\perp}$  is a real quantity, and evanescent field components to the case where  $q_{\perp}$  is a purely imaginary quantity. If we want to get a broad understanding of the phase conjugated response of a probe containing both propagating and evanescent field components from a quantum-well phase conjugator, two cases are of fundamental interest, namely, (i) the pure intraband case and (ii) the case where also an interband transition is involved.

The phase conjugated response from a pure intraband quantum well we have described in Ref. 49. This analysis revealed that the phase conjugation reflection coefficient is not only highly nonuniform in the  $\mathbf{q}_{\parallel}$  spectrum, but also that the coupling efficiency is several orders of magnitude larger in part of the evanescent regime than in the propagating regime. Since evanescent waves are strongly decaying in space we further concluded that if one wants to see the phase conjugation of evanescent modes, both excitation and observation should take place close to the surface of the quantum well. Furthermore was discussed the problems of excitation of the near-field regime, and the consequences from choosing a broad banded (with respect to  $\mathbf{q}_{\parallel}$ ) two-dimensional point source (quantum wire) revealed that parts of the evanescent spectrum could be excited, and in Ref. 71 that phase conjugation of evanescent fields can lead to a focus of the phase conjugated field substantially below the so-called diffraction limit.<sup>72,73</sup> Since this has also been experimentally observed,<sup>74</sup> we judge that it is highly relevant also to give an account of how evanescent fields are phase conjugated in a system where not only one electronic level is present.

Since including more than one interband transition will be necessary for most practical applications, we present in this paper the complete solution to the theoretical model of Ref. 58 in the case of two-dimensional translational invariance, although a description based on the self-field approximation according to the Fiebelman theory<sup>75,76</sup> would be sufficient in order to determine the dominating response. Giving a complete solution also allows us to comment on what we would lose using the self-field approximation. The solution is based on a discretization in the energy levels of the two-dimensionally translational invariant medium. Contrary to discretization schemes performed in real space or Fourier space, our discretization does not in itself imply an approximation. Thus, once the complete orthonormal set of wave functions for the phase conjugating medium has been determined, the phase conjugated response can in principle be calculated from the solution presented in this paper. How to find the proper set of wave functions for a given material system is another problem, which for example can be treated using one of several band-structure methods,<sup>77,78</sup> e.g., the Korringa-Kohn-Rostoker (KKR),<sup>79,80</sup> the linearized augmented plane-wave (LAPW),<sup>81</sup> or the linear muffin-tin orbital (LMTO) method.<sup>82</sup> These methods are based on an atomic description of the potential in a certain radius of each atom, adding exchange and correlation terms<sup>83</sup> and different approximations in the regions between the atomic boundaries. Using such a method one will probably be able to give more accurate numerical results for specific materials, but at the cost of the (relatively) analytical simplicity. Therefore, we will not elaborate further on this point here, but in stead

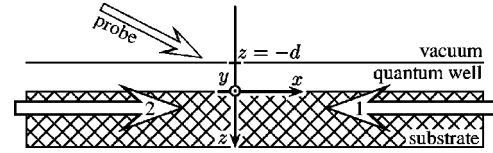


FIG. 1. The system we consider here consists of a three layer structure, namely, (i) vacuum, extending from  $-\infty$  to  $-d$ , (ii) quantum well, extending from  $-d$  to  $0$ , and (iii) substrate (cross hatched), extending from  $0$  to  $+\infty$ . The three incoming electromagnetic fields consists of two pump fields (labeled 1 and 2) and a probe field. Also shown is the Cartesian coordinate system used in our calculations.

resort to using a simple description of the matter wave functions. Doing so, we will be able to present a qualitative discussion based on analytical expressions.

Using a two-level quantum-well phase conjugator, it is also possible to study resonant four-wave mixing, which until now has been studied only without spatial dispersion [at the point  $(q_{\parallel}, \omega) = (0, \omega_{21})$  in the  $q_{\parallel}-\omega$  plane,  $\omega_{21}$  being the interband transition frequency], as described in, e.g., Refs. 84–87. Thus, in Sec. II we present the theory in the form of a local-field formalism, we choose a scattering geometry, and the solution is presented as a discretization in the energy eigenstates. In Sec. III we prepare for a numerical calculation. We start by adopting the simple infinite barrier (IB) model to describe the quantum well. Furthermore we define the phase conjugation reflection coefficient, and the section is concluded with a specific choice of a convenient system to investigate. To give an impression of the implications of our theoretical model we have presented in Sec. IV numerical calculations for a two-level quantum-well phase conjugator. The calculation is supplemented by a discussion of the results, in particular an identification of the different resonances appearing when the wave number along the surface plane as well as the frequency varies. In Sec. V we widen our discussions, with emphasis on (i) the interband resonance, (ii) the validity of the self-field approximation, and (iii) the choice of appropriate relaxation times. Finally, in Sec. VI, we conclude.

## II. THEORY

As a forerunner for the analysis of the optical phase conjugation from a two-level quantum well we briefly sketch how a local-field calculation allows one to determine the so-called degenerate four-wave mixing response of a mesoscopic metallic film deposited on a dielectric substrate. To create a phase conjugated field, which in the plane of the film propagates in a direction opposite to that of the probe field, two counterpropagating pump fields must be present inside the phase conjugating medium. Although the theoretical model developed in Ref. 58 allows us to make almost arbitrary choices of the interacting optical fields, we will in the present work assume for simplicity that the pump fields (i) propagate parallel to the plane of the film and (ii) have constant amplitude across the film. The scattering geometry is shown in Fig. 1 together with the chosen coordinate system. We will further limit our study to the case where (iii) scattering takes place in the  $x-z$  plane and (iv) the interacting fields are linearly polarized, either in ( $p$  polarized) or perpen-

dicular to ( $s$  polarized) the scattering plane. Since it is necessary in a study of nonlinear optical phenomena in mesoscopic interaction volumes to abandon macroscopic electrodynamics, the starting point is the microscopic Maxwell-Lorentz equations. The phase conjugated field from a quantum well exhibiting free-electron-like dynamics in the plane of the well ( $x$ - $y$  plane) can then be described using the single-coordinate ( $z$ ) loop equation<sup>88</sup>

$$\begin{aligned} \mathbf{E}_{PC}(z; \mathbf{q}_{\parallel}, \omega) = & \mathbf{E}_{PC}^B(z; \mathbf{q}_{\parallel}, \omega) - i\mu_0\omega \int \int \vec{G}(z, z''; \mathbf{q}_{\parallel}, \omega) \\ & \cdot \vec{\sigma}(z'', z'; \mathbf{q}_{\parallel}, \omega) \cdot \mathbf{E}_{PC}(z'; \mathbf{q}_{\parallel}, \omega) dz'' dz', \end{aligned} \quad (1)$$

where  $\omega$  is the common angular frequency of the participating fields and  $\mathbf{q}_{\parallel}$  is the component of the probe field in the film plane. It is the so-called background field  $\mathbf{E}_{PC}^B(z; \mathbf{q}_{\parallel}, \omega)$  which makes the loop problem different for the various nonlinear (and linear) problems. It is here given by

$$\mathbf{E}_{PC}^B(z; \mathbf{q}_{\parallel}, \omega) = -i\mu_0\omega \int \vec{G}(z, z'; \mathbf{q}_{\parallel}, \omega) \cdot \mathbf{J}_{-\omega}^{(3)}(z'; \mathbf{q}_{\parallel}, \omega) dz', \quad (2)$$

where  $\mathbf{J}_{-\omega}^{(3)}(z'; \mathbf{q}_{\parallel}, \omega)$  is the current density driving the nonlinear process. The pseudovacuum propagator  $\vec{G}(z, z''; \mathbf{q}_{\parallel}, \omega)$  is given by

$$\begin{aligned} \vec{G}(z, z'; \mathbf{q}_{\parallel}, \omega) = & \frac{e^{iq_{\perp}|z-z'|}}{2iq_{\perp}} [\mathbf{e}_y \otimes \mathbf{e}_y + \Theta(z-z') \mathbf{e}_i \otimes \mathbf{e}_i \\ & + \Theta(z'-z) \mathbf{e}_r \otimes \mathbf{e}_r] + \frac{e^{-iq_{\perp}(z+z')}}{2iq_{\perp}} [r^s \mathbf{e}_y \otimes \mathbf{e}_y \\ & + r^p \mathbf{e}_r \otimes \mathbf{e}_r] + \frac{1}{q^2} \delta(z-z') \mathbf{e}_z \otimes \mathbf{e}_z, \end{aligned} \quad (3)$$

where the first term describes the direct propagation of the electromagnetic field from a source plane at  $z'$  to the observation plane at  $z$ , the second term accounts for the reflection at the quantum-well-substrate interface, and the third term characterizes the field generated at the observation plane by the current density prevailing in the same plane (thus named the self-field term). Above,  $\mathbf{e}_i = q^{-1}(q_{\perp}, 0, -q_{\parallel})$ , and  $\mathbf{e}_r = q^{-1}(-q_{\perp}, 0, -q_{\parallel})$ , taking  $\mathbf{q}_{\parallel} = q_{\parallel} \mathbf{e}_x$ . The quantities  $r^s$  and  $r^p$  are the amplitude reflection coefficients at the vacuum-substrate interface in the absence of the quantum well for  $s$ - and  $p$ -polarized fields, respectively. Both of these are in general functions of  $q_{\parallel}$ . Moreover, the vectors  $\mathbf{e}_x$ ,  $\mathbf{e}_y$ , and  $\mathbf{e}_z$  are unit vectors along the principal axes in the Cartesian  $x$ - $y$ - $z$ -coordinate system,  $\Theta(\cdots)$  is the Heaviside unit step function and  $\delta(\cdots)$  is the Dirac delta function.

The  $ij$ th tensor element of the linear response tensor  $\vec{\sigma}(z'', z'; \mathbf{q}_{\parallel}, \omega)$ , appearing in Eq. (1), is given by<sup>88,89</sup>

$$\begin{aligned} \sigma_{ij}(z, z'; \mathbf{q}_{\parallel}, \omega) = & \frac{2i}{\hbar\omega} \frac{1}{(2\pi)^2} \sum_{nm} \int \frac{\omega}{\tilde{\omega}_{nm}(\boldsymbol{\kappa}_{\parallel} + \mathbf{q}_{\parallel}, \boldsymbol{\kappa}_{\parallel})} \\ & \times \frac{f_n(\boldsymbol{\kappa}_{\parallel} + \mathbf{q}_{\parallel}) - f_m(\boldsymbol{\kappa}_{\parallel})}{\tilde{\omega}_{nm}(\boldsymbol{\kappa}_{\parallel} + \mathbf{q}_{\parallel}, \boldsymbol{\kappa}_{\parallel}) - \omega} \\ & \times j_{i, nm}(z; 2\boldsymbol{\kappa}_{\parallel} + \mathbf{q}_{\parallel}) \\ & \times j_{j, mn}(z'; 2\boldsymbol{\kappa}_{\parallel} + \mathbf{q}_{\parallel}) \end{aligned} \quad (4)$$

provided the set of wave functions is complete. In Eq. (4) we have introduced the transition current density in the mixed Fourier space, namely,

$$\begin{aligned} \mathbf{j}_{nm}(z; \mathbf{Q}_{\parallel}) = & -\frac{e\hbar}{2im_e} \left[ i\mathbf{Q}_{\parallel} \psi_m^*(z) \psi_n(z) + \mathbf{e}_z \left( \psi_m^*(z) \frac{d\psi_n(z)}{dz} \right. \right. \\ & \left. \left. - \psi_n(z) \frac{d\psi_m^*(z)}{dz} \right) \right]. \end{aligned} \quad (5)$$

In relation to Eq. (4),  $\mathbf{Q}_{\parallel}$  is equal to  $2\boldsymbol{\kappa}_{\parallel} + \mathbf{q}_{\parallel}$ , where  $\boldsymbol{\kappa}_{\parallel}$  is the wave vector of the given electron in the plane of the well. The transition current density also occurs in the nonlinear response tensor (see Appendix A) and in this context various combinations of  $\mathbf{q}_{\parallel}$ ,  $\mathbf{k}_{\parallel}$ , and  $\boldsymbol{\kappa}_{\parallel}$  appear in  $\mathbf{Q}_{\parallel}$ . The quantities  $\psi_a$ ,  $a \in \{n, m\}$ , are the one-dimensional electronic energy eigenstates of the quantum well belonging to the  $z$  direction, and they satisfy the field-unperturbed Schrödinger equation  $\mathcal{H}_0 \psi_a = \varepsilon_a \psi_a$ . The quantity  $f_a(\boldsymbol{\kappa}_{\parallel})$  denote the Fermi-Dirac distribution for the eigenstate  $\Psi_a(\mathbf{r}) = \psi_a(z) \exp(i\boldsymbol{\kappa}_{\parallel} \cdot \mathbf{r}) / (2\pi)$ , where also the solution to the Schrödinger equation along the quantum well is taken into account. It is given by  $f_a(\boldsymbol{\kappa}_{\parallel}) = [1 + \exp\{(\varepsilon_a + \hbar^2 \boldsymbol{\kappa}_{\parallel}^2 / (2m_e) - \mu) / (k_B T)\}]^{-1}$ , where  $k_B$  is the Boltzmann constant,  $\mu$  is the chemical potential of the electron system, and  $T$  the absolute temperature. For the various Cartesian components of the transition current density, we use the notation  $j_{i, nm}(z; \boldsymbol{\kappa}_{\parallel})$ ,  $i \in \{x, y, z\}$ . The complex cyclic transition frequency is defined by

$$\begin{aligned} \tilde{\omega}_{nm}(\mathbf{Q}_{\parallel, a}, \mathbf{Q}_{\parallel, b}) = & \frac{1}{\hbar} \left[ \varepsilon_n - \varepsilon_m + \frac{\hbar^2}{2m_e} (|\mathbf{Q}_{\parallel, a}|^2 - |\mathbf{Q}_{\parallel, b}|^2) \right] \\ & - i\tau_{nm}^{-1}, \end{aligned} \quad (6)$$

where  $\varepsilon_n$  and  $\varepsilon_m$  are the eigenenergies of the quantum well states belonging to the  $z$  direction, and  $\mathbf{Q}_{\parallel, a}$  and  $\mathbf{Q}_{\parallel, b}$  can be any of the relevant combinations of  $\mathbf{q}_{\parallel}$ ,  $\mathbf{k}_{\parallel}$ , and  $\boldsymbol{\kappa}_{\parallel}$ . The quantity  $\tau_{nm}$  is the relaxation time.

The nonlinear current density,  $\mathbf{J}_{-\omega}^{(3)}(z'; \mathbf{q}_{\parallel}, \omega)$ , is related to the pump and probe fields by a constitutive relation of the form

$$\begin{aligned} \mathbf{J}_{-\omega}^{(3)}(z; \mathbf{q}_{\parallel}, \omega) = & \frac{1}{(2\pi)^4} \int \int \vec{\Xi}(z, z'; \mathbf{q}_{\parallel}, \mathbf{k}_{\parallel}, \omega) \dot{\mathbf{E}}(-\mathbf{k}_{\parallel}, \omega) \\ & \times \mathbf{E}(\mathbf{k}_{\parallel}, \omega) \mathbf{E}^*(z'; -\mathbf{q}_{\parallel}, \omega) dz' + i.t., \end{aligned} \quad (7)$$

where

$$\vec{\Xi}(z, z'; \mathbf{q}_{\parallel}, \mathbf{k}_{\parallel}, \omega) = \int \int \vec{\Xi}(z, z', z'', z'''; \mathbf{q}_{\parallel}, \mathbf{k}_{\parallel}, \omega) dz'' dz''' \quad (8)$$

is the relevant nonlinear response tensor when the pump fields are essentially constant (slowly varying) across the quantum well, i.e.,  $\mathbf{E}(z''; -\mathbf{k}_\parallel, \omega) = \mathbf{E}(-\mathbf{k}_\parallel, \omega)$  and  $\mathbf{E}(z''; \mathbf{k}_\parallel, \omega) = \mathbf{E}(\mathbf{k}_\parallel, \omega)$  in Eq. (7). Within the framework of a single-electron random-phase-approximation approach an explicit expression for  $\tilde{\Xi}(z, z', z'', z'''; \mathbf{q}_\parallel, \mathbf{k}_\parallel, \omega)$  has been established in Ref. 58. The term ‘‘i.t.’’ denotes the so-called ‘‘interchanged term,’’ which takes into account the symmetry of the pump fields. It is obtained from the first term by interchanging the two pump fields (the pump field wave vector  $\mathbf{k}_\parallel$  is replaced by  $-\mathbf{k}_\parallel$ ). The explicit expression for the simplified nonlinear conductivity tensor,  $\tilde{\Xi}(z, z'; \mathbf{q}_\parallel, \mathbf{k}_\parallel, \omega)$ , can be found in Appendix A. We have, however, in Appendix A only listed one of the seven parts, namely, part *G*, of the nonlinear conductivity tensor that appears in Ref. 58, since when interband transitions are strong, it is dominating the response by several orders of magnitude compared to the other six (*A–F*).

As a consequence of the above-mentioned choice (but independent of the direction in which the pump fields propagate) the number of terms in the nonvanishing elements of the nonlinear response tensor is further reduced, since the orthonormality of the *z*-dependent parts of the wave function gives

$$\int \psi_n^*(z) \psi_m(z) dz = \delta_{nm}, \quad (9)$$

where  $\delta_{nm}$  is the Kronecker delta. Also, by integration of the microscopic transition current density given by Eq. (5) over *z* one finds

$$\int \mathbf{j}_{nm}(z; \mathbf{Q}_\parallel) dz = -\frac{e\hbar}{2im_e} [i\mathbf{Q}_\parallel \delta_{nm} + p_{z,nm} \mathbf{e}_z], \quad (10)$$

where

$$p_{z,nm} = \int \left( \psi_m^*(z) \frac{d\psi_n(z)}{dz} - \psi_n(z) \frac{d\psi_m^*(z)}{dz} \right) dz \quad (11)$$

is proportional to the *z* component of the electric dipole moment related to the *nm* transition.<sup>90</sup>

The conductivity tensor  $\tilde{\Xi}(z, z', z'', z'''; \mathbf{q}_\parallel, \mathbf{k}_\parallel, \omega)$  has in general 81 nonzero tensor elements ( $3 \times 3 \times 3 \times 3$ ) and consists of seven different parts (*A–G*) after the seven different physical processes contributing to the response (see Ref. 58 for details). When scattering takes place in the *x–z* plane with linearly polarized light the general treatment can be split into eight separate parts related to the possible combinations of polarization of the three different incident fields. In this scattering geometry  $\mathbf{q}_\parallel$  and  $\mathbf{k}_\parallel$  lie along the *x* axis, giving a mirror plane at *y*=0. Consequently, only tensor elements in the nonlinear response tensor with a Cartesian index even numbered in *y* contributes, and the 81 tensor elements generally appearing are reduced to 41. The separation of the tensor elements into the eight sets of elements contributing in these configurations follows in a straight forward manner from the definition of the sum-product operator ‘‘:’’ between the nonlinear current density and the interacting electric fields, i.e.,  $[\tilde{\Xi} : \mathbf{E}\mathbf{E}\mathbf{E}^*]_i = \sum_{jkh} \Xi_{ijkh} E_h E_k E_j^*$ . The added restriction of letting the pump fields travel along

TABLE I. Contributing tensor elements of the nonlinear conductivity tensor when the pump fields are propagating in the *x* direction and all fields are polarized in (*p*) or perpendicular to (*s*) the *x–z* plane. The left column shows the polarization combination of the incoming fields (pump 1, pump 2, probe), the center columns shows the polarization of the phase conjugated field, and the right column shows the tensor elements contributing to the nonlinear interaction.

input pol.	output pol.	nonlinear tensor elements
<i>sss</i>	<i>s</i>	$\Xi_{yyyy}$
<i>pps</i>	<i>s</i>	$\Xi_{yyzz}$
<i>ssp</i>	<i>p</i>	$\Xi_{xxyy}, \Xi_{xzzy}, \Xi_{zxyy}, \Xi_{zzyy}$
<i>ppp</i>	<i>p</i>	$\Xi_{xxzz}, \Xi_{xzxx}, \Xi_{zxzz}, \Xi_{zzzz}$
<i>spp, psp</i>	<i>s</i>	$\Xi_{yxyz}, \Xi_{yxzy}, \Xi_{zyyz}, \Xi_{yzzy}$
<i>sp, pss</i>	<i>p</i>	$\Xi_{xyyz}, \Xi_{xyzy}, \Xi_{zyyz}, \Xi_{zyzy}$

the *x* axis then reduces the number of contributing matrix elements from 41 to 18, since when traveling along the *x* axis, the pump fields are polarized in either the *y* direction or the *z* direction. The resulting sets of tensor elements we have presented in Table I.

To solve Eq. (1), we can establish a so-called coupled antenna loop. First, we notice that each matrix element of the linear conductivity tensor [Eq. (4)] with the insertion of Eq. (5) can be written as a product of a *z*-independent term and two terms depending on *z* and *z'*, respectively. Element *ij* then takes the form

$$\sigma_{ij}(z, z'; \mathbf{q}_\parallel, \omega) = \sum_{nm} Q_{nm}^{ij}(\mathbf{q}_\parallel, \omega) j_{i,nm}(z) j_{j,mn}(z'), \quad (12)$$

where  $\mathbf{j}_{nm}(z) \equiv \mathbf{j}_{nm}(z; \mathbf{e}_x + \mathbf{e}_y)$ . The various *Q* quantities can readily be identified from Eq. (4), and the integrals can be solved using the method described in Appendix B. Inserting Eq. (12) into Eq. (1), we get

$$\mathbf{E}_{PC}(z) = \mathbf{E}_{PC}^B(z) + \sum_{nm} \vec{F}_{nm}(z) \cdot \mathbf{\Gamma}_{mn}, \quad (13)$$

omitting the reference to  $\mathbf{q}_\parallel$  and  $\omega$  for brevity. In Eq. (13) we have introduced the  $3 \times 3$  tensor  $\vec{F}_{nm}(z)$  with the nonzero elements

$$\begin{aligned} F_{nm}^{xx}(z) &= -i\mu_0\omega \sum_{i \in \{x,z\}} Q_{nm}^{xi} \int G_{xi}(z, z'') j_{i,nm}(z'') dz'' \\ &= \frac{q_\perp}{q_\parallel} F_{nm}^{zx}(z), \end{aligned} \quad (14)$$

$$\begin{aligned} F_{nm}^{xz}(z) &= -i\mu_0\omega \sum_{i \in \{x,z\}} Q_{nm}^{iz} \int G_{xi}(z, z'') j_{i,nm}(z'') dz'' \\ &= \frac{q_\perp}{q_\parallel} F_{nm}^{zz}(z), \end{aligned} \quad (15)$$

$$F_{nm}^{yy}(z) = -i\mu_0\omega Q_{nm}^{yy} \int G_{yy}(z, z'') j_{y,nm}(z'') dz'', \quad (16)$$

and the elements of the vector  $\mathbf{\Gamma}_{mn}$  are written

$$\Gamma_{i,mn} = \int j_{i,mn}(z') E_{PC,i}(z') dz', \quad i \in \{x, y, z\}. \quad (17)$$

To determine the phase conjugated field the quantity  $\Gamma_{mn}$  must be calculated. This is done by multiplication of each element  $E_{PC,i}(z')$ ,  $i \in \{x, y, z\}$  of the phase conjugated field in Eq. (1) by the relevant  $j_{i,mn}(z)$  followed by an integration over the  $z$  coordinate. Hence, when the phase conjugated light is  $s$  polarized, Eq. (13) is transformed into the following set of linear algebraic equations:

$$\Gamma_{y,mn} - \sum_{vl} K_{yy,mn}^{vl} \Gamma_{y,vl} = \Omega_{y,mn}, \quad (18)$$

i.e.,  $n^2$  equations with just as many unknowns. In the case of  $p$ -polarized light, we obtain

$$\Gamma_{x,mn} - \sum_{vl} (K_{xx,mn}^{vl} \Gamma_{x,vl} + K_{xz,mn}^{vl} \Gamma_{z,vl}) = \Omega_{x,mn}, \quad (19)$$

$$\Gamma_{z,mn} - \sum_{vl} (K_{zx,mn}^{vl} \Gamma_{x,vl} + K_{zz,mn}^{vl} \Gamma_{z,vl}) = \Omega_{z,mn}, \quad (20)$$

which are  $2n^2$  equations with just as many unknowns. In Eqs. (18)–(20) above, the elements of the vectorial quantity  $\Omega_{mn}$  are given by

$$\Omega_{i,mn} = \int j_{i,mn}(z) E_{PC,i}^B(z) dz, \quad i \in \{x, y, z\}, \quad (21)$$

and the  $3 \times 3$  tensorial quantity  $\vec{K}_{mn}^{vl}(\mathbf{q}_{\parallel}, \omega)$  has the five non-zero elements

$$K_{ij,mn}^{vl} = \int j_{i,mn}(z) F_{lv}^{ij}(z) dz, \quad (22)$$

where the indices “ $i$ ” and “ $j$ ” can take the values of  $ij \in \{xx, xz, yy, zx, zz\}$ . By means of the procedure sketched above, we have been able to transform the integral-equation problem for the phase conjugated field  $\mathbf{E}_{PC}(z)$ , [Eq. (1)] to a matrix problem for the  $\Gamma_{mn}$  vectors. This discretization in the energy levels is exact, and once the linear algebraic set of equations for the  $\Gamma_{mn}$  vectors, truncated so as to keep only the subspace of relevant energy levels, has been solved (numerically) the phase conjugated field can be obtained from Eq. (13). Integral equations of the type given in Eq. (1) is often solved (numerically) by discretization in the real space coordinate. By such a procedure one has to worry about how small discretization lengths one may dare to take from a physical point of view. The discretization in energy levels used here does not suffer from this uncertainty.

### III. NUMERICAL FRAMEWORK

Our description of the phase conjugated field has until now been independent of the actual wave functions in the quantum well, and thus also independent of the form the potential takes across the active medium. However, if we want to perform a numerical calculation of the phase conjugated field we have to choose a definite potential across the quantum well, giving us a set of wave functions to work with. Below we use the infinite barrier (IB) model potential

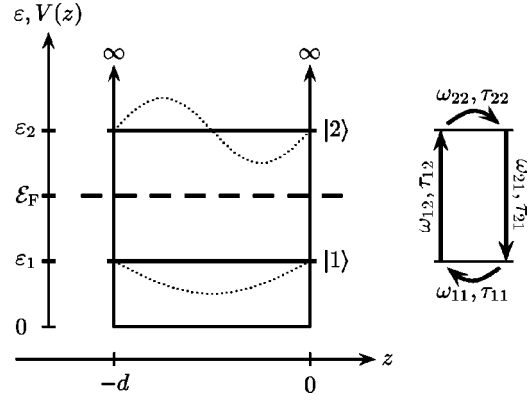


FIG. 2. Infinite barrier (IB) model potential (thick solid line) for a quantum well with boundaries at  $z = -d$  and  $z = 0$ . In the present case, only one energy level below the Fermi energy (here called |1>, with energy  $\varepsilon_1$ ) and one energy level above the Fermi energy (called |2>, with energy  $\varepsilon_2$ ) contributes to the solution. The remaining infinite set of energies appearing in the IB model we assume are so far away from |1> and |2> that they do not contribute to the solution. The dotted curves indicate the shape of the wave function for each of the two energies. To the right is shown the possible transitions, identified with their respective transition frequency and relaxation time.

for the numerical study, since this model is sufficient for a qualitative study.

As shown in Fig. 2, in this model the one-dimensional potential  $V(z)$  is zero inside the quantum well (in the interval  $-d \leq z \leq 0$ ) and infinite everywhere else. The stationary state wave functions inside the quantum well are given by  $\psi_n(z) = \sqrt{2/d} \sin(n\pi z/d)$  and outside the quantum well,  $\psi_n(z) = 0$ . The associated eigenenergies are  $\varepsilon_n = (n\pi\hbar)^2 / (2m_e d^2)$ . Within the IB model, Eq. (11) gives

$$p_{z,nm} = \frac{4nm[1 - (-1)^{n+m}]}{(n^2 - m^2)d} \quad (23)$$

for  $n \neq m$ , and  $p_{z,nm} = 0$  for  $n = m$ . For a metallic quantum well one may even at room temperature approximate the Fermi-Dirac distribution functions by their value at zero temperature, i.e.,

$$\lim_{T \rightarrow 0} f_n(\kappa_{\parallel}) = \Theta \left\{ \mathcal{E}_F - \frac{\hbar^2}{2m_e} \left[ \left( \frac{n\pi}{d} \right)^2 + \kappa_{\parallel}^2 \right] \right\}, \quad (24)$$

where  $\mathcal{E}_F$  is the Fermi energy of the system. In the low-temperature limit it is possible to find analytical solutions to the integrals over  $\kappa_{\parallel}$  appearing in Eq. (A1). The explicit calculations are tedious but trivial to carry out, and since the final expressions are rather long we do not present them here. For the interested reader some steps in the calculations are reproduced in Appendix B.

The Fermi energy is calculated from the global charge neutrality condition,<sup>88</sup> and for a quantum well described by the IB model, it becomes<sup>89</sup>

$$\mathcal{E}_F = \frac{\pi\hbar^2}{N_F m_e} \left[ ZN_+ d + \frac{\pi}{2d^2} \frac{N_F(N_F + 1)(2N_F + 1)}{6} \right], \quad (25)$$

where  $N_+$  is the number of positive ions per unit volume,  $Z$  is the valence of these ions, and  $N_F$  is the quantum index of

the highest occupied level. From Eq. (25), the number of occupied levels can be calculated if the thickness is known, and vice versa. The minimal thickness for the quantum well to have  $n$  levels below the Fermi level can be determined from the relation  $\mathcal{E}_F = \varepsilon_n$ , and the maximal thickness from the condition  $\mathcal{E}_F = \varepsilon_{n+1}$ . Thus for  $n$  bound states below the Fermi energy we find the minimal and maximal thicknesses

$$d_{\min}^n = d_{\max}^{n-1} = \sqrt[3]{\frac{\pi n}{2ZN_+} \left[ n^2 - \frac{(n+1)(2n+1)}{6} \right]}, \quad (26)$$

i.e., a result that depends on the number of levels below the Fermi energy and the number of conduction electrons in the film.

To estimate the amount of phase conjugated light, we use the phase conjugation (energy) reflection coefficient defined as

$$R_{PC}(\mathbf{q}_{\parallel}, \omega) = \frac{I_{PC}(-d; \mathbf{q}_{\parallel}, \omega)}{I^{(1)} I^{(2)} I_{\text{probe}}(-d; \mathbf{q}_{\parallel}, \omega)}, \quad (27)$$

in which  $I^{(1)}$ ,  $I^{(2)}$ ,  $I_{\text{probe}}$ , and  $I_{PC}$  are the intensities of the two pump beams, the probe and the phase conjugated field, respectively. Each of the intensities are given by  $I = (1/2)\varepsilon_0 c_0 \mathbf{E} \cdot \mathbf{E}^* (2\pi)^{-4}$ . The factor of  $(2\pi)^{-4}$  originates from the manner in which we have introduced the Fourier amplitudes of the fields.

For the remaining part of this work we choose a copper quantum well with  $N_+ = 8.47 \times 10^{28} \text{ m}^{-3}$  and  $Z = 1$  (data taken from Ref. 91). The Cu quantum well is assumed to be deposited on a glass substrate for which we use a refractive index  $n$  of 1.51. With this substrate, the linear vacuum-substrate amplitude reflection coefficients can be obtained by use of the classical Fresnel formulas  $r^s = [q_{\perp} - (n^2 q^2 - q_{\parallel}^2)^{1/2}] / [q_{\perp} + (n^2 q^2 - q_{\parallel}^2)^{1/2}]$  and  $r^p = [n^2 q_{\perp} - (n^2 q^2 - q_{\parallel}^2)^{1/2}] / [n^2 q_{\perp} + (n^2 q^2 - q_{\parallel}^2)^{1/2}]$ . Having the pump wavevectors parallel to the  $x$  axis then gives a pump wave-number of  $k_{\parallel} = nq = 1.51q$ .

#### IV. NUMERICAL RESULTS FOR A TWO-LEVEL QUANTUM WELL

To calculate the phase conjugated response from a quantum well with an arbitrary number of bound eigenstates one would have to superimpose interband and intraband contributions. Thus in a study of the complete response where local-field effects are neglected one basically would have to add the contributions from the various pairs of levels located in different subbands or in the same band. Seen in this light, thorough treatments of the single-level case, where only intraband transitions are allowed, and the two-level case, where transitions between two eigenstates located in different bands occur, would form a good qualitative starting point for analyses of multilevel quantum-well systems. The single-level case we have studied before,<sup>49</sup> and the following treatment will thus be directed towards a description of the phase conjugated response from a two-level quantum well. Thus, we choose the simplest possible configuration in which interband transitions can occur, i.e., a quantum well with only one bound state below the Fermi energy. Above the Fermi energy we also assume that only one bound state can be reached, and thus the wave functions are  $\psi_1(z)$

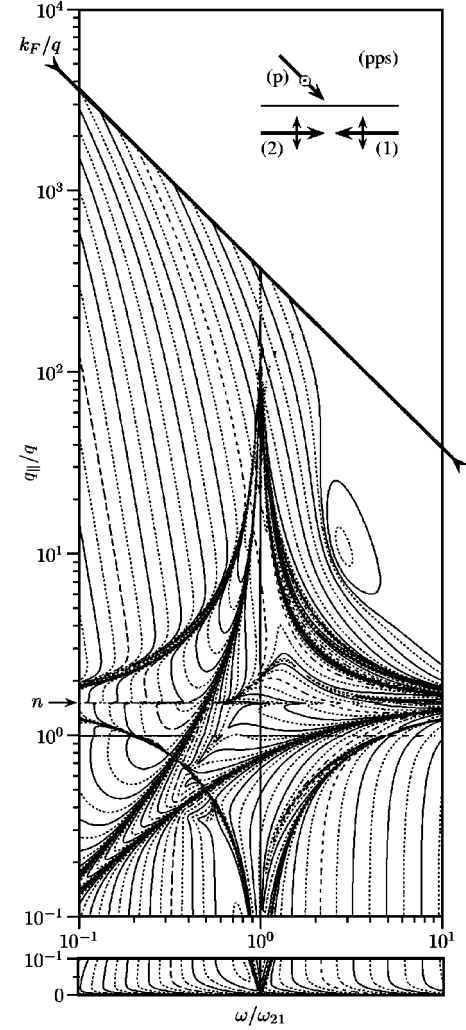


FIG. 3. The phase conjugation reflection coefficient from a two-level metallic quantum well is plotted in the case where  $s$ -polarized probe field gives  $s$ -polarized phase conjugated response, and where the pump fields are  $p$  polarized ( $pps$ ). The response is plotted as isophotes (contours of equal intensity)  $[\text{m}^4/\text{W}^2]$  on a logarithmic scale as a function of (i) the frequency  $\omega$  normalized to the transition frequency  $\omega_{21}$  and (ii) the parallel component of the wave vector, normalized to the vacuum wave number. The difference between two neighboring contours is one order of magnitude. To indicate the absolute amplitude, the isophote of value  $10^{-20} \text{ m}^4/\text{W}^2$  has been plotted using a long-dashed curve and the isophote with magnitude  $10^{-30} \text{ m}^4/\text{W}^2$  with a short-dashed curve. On the  $q_{\parallel}/q$  scale, the response has been plotted on a linear scale in the range  $0 \leq q_{\parallel}/q \leq 0.1$  and on a logarithmic scale above  $q_{\parallel}/q = 0.1$ .

$= \sqrt{2/d} \sin(\pi z/d)$  and  $\psi_2(z) = \sqrt{2/d} \sin(2\pi z/d)$ . The associated energies then become  $\varepsilon_1 = (\pi\hbar)^2/(2m_e d^2)$ , and  $\varepsilon_2 = (2\pi\hbar)^2/(2m_e d^2)$ , respectively. The quantum well with the various relevant energies and wave functions, as well as the electronic excitations are shown in schematic form in Fig. 2. In the present two-level case Eq. (23) becomes

$$p_{z,nm} = \frac{16}{3d} \text{sgn}(n-m), \quad (28)$$

where  $(n, m) \in \{(1,2), (2,1)\}$ . If just the ground state should have an energy less than the Fermi energy, we see from Eq.

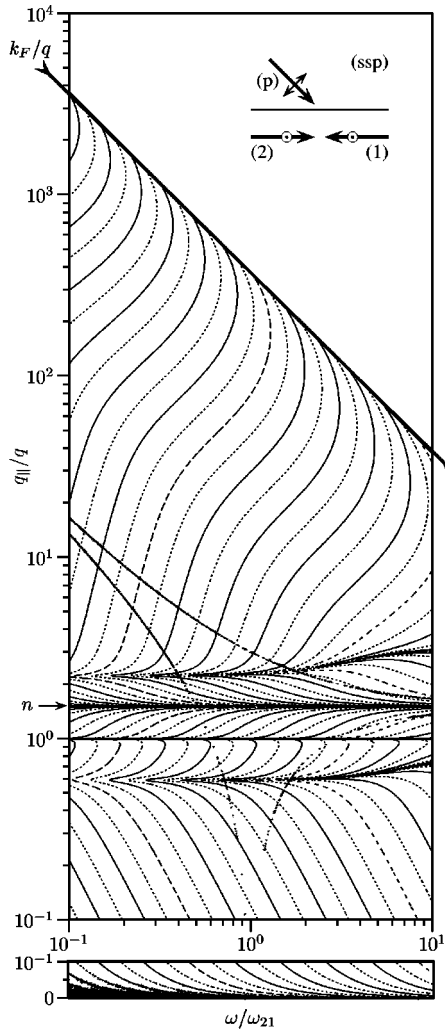


FIG. 4. The phase conjugation reflection coefficient from a two-level metallic quantum well is plotted in one of the cases where  $p$ -polarized probe field gives  $p$ -polarized phase conjugated response. In this case the pump fields are  $s$ -polarized (thus named  $spp$ ). The response is plotted as isophotes [ $\text{m}^4/\text{W}^2$ ] on a logarithmic scale as a function of (i) the frequency  $\omega$  normalized to the transition frequency  $\omega_{12}$  and (ii) the parallel component of the wave vector, normalized to the vacuum wave number. The difference between two neighboring isophotes is one order of magnitude. Again, the two isophotes of magnitude  $10^{-20}$  and  $10^{-30} \text{ m}^4/\text{W}^2$  has been plotted with long- and short-dashed curves, respectively. As before, below 0.1,  $q_{\parallel}/q$  has been plotted on a linear scale while above it is logarithmic.

(26) that the film thickness must be less than  $d_{\max} = \sqrt[3]{3\pi/(2ZN_+)}$ . The minimal thickness is in the IB model zero, but in reality the smallest thickness is a single monolayer. Using Eq. (26) the maximal thickness for a two-level Cu quantum well then becomes  $d_{\max} \approx 3.82 \text{ \AA}$ , which is more than two monolayers and less than three. Thus we have two obvious choices for the thickness of the quantum well, namely, a single monolayer or two monolayers. We choose two monolayers, since by this choice the two energies  $\varepsilon_1$  and  $\varepsilon_2$  are closest to each other, and thus the energy needed for a resonant transition to occur is lowest. Two monolayers of copper roughly corresponds to a thickness of  $d = 3.6 \text{ \AA}$  (bulk value). With this choice, the energy difference between the

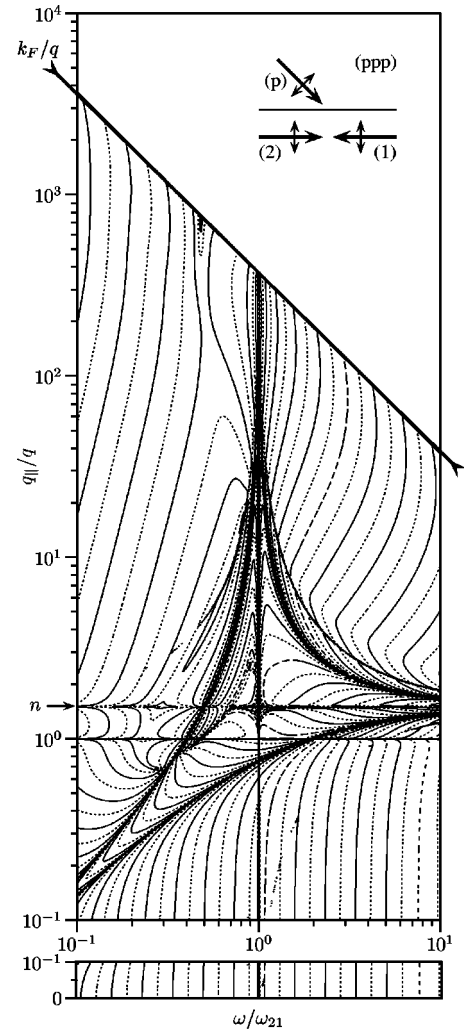


FIG. 5. The phase conjugation reflection coefficient from a two-level metallic quantum well is plotted in the other case where  $p$ -polarized probe field gives  $p$ -polarized phase conjugated response, this time with  $p$ -polarized pump fields ( $ppp$ ). As in Figs. 4 and 5, the response is plotted as isophotes [ $\text{m}^4/\text{W}^2$ ] on a logarithmic scale as a function of (i) the frequency  $\omega$  normalized to the transition frequency  $\omega_{12}$  and (ii) the parallel component of the wave vector, normalized to the vacuum wave number. Again, the difference between two neighboring contours is one order of magnitude, and as before, the long- and short-dashed curves represents magnitudes of  $10^{-20}$  and  $10^{-30} \text{ m}^4/\text{W}^2$ , respectively. In the big picture,  $q_{\parallel}/q$  is plotted on a logarithmic scale, while in the strip it is plotted on a linear scale.

two states is  $\varepsilon_2 - \varepsilon_1 = 8.70 \text{ eV}$ , and the corresponding resonance in the optical spectrum is found at the wavelength  $\lambda = 142.4 \text{ nm}$ .

#### A. Phase conjugation reflection coefficient

Among the eight possible ways of using linearly polarized light in our chosen scattering configuration, two combinations give an  $s$ -polarized response when using an  $s$ -polarized probe field, the pump fields being either  $s$  polarized or  $p$  polarized, but with the same polarization for both pump fields. When the pump fields are  $s$ -polarized, the nonlinear conductivity tensor element that contributes to the response

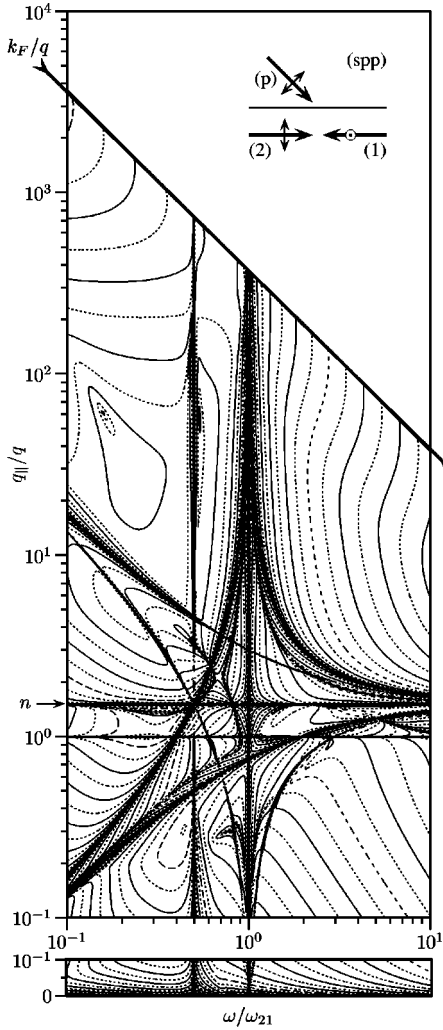


FIG. 6. The phase conjugation reflection coefficient from a two-level metallic quantum well is plotted in one of the cases where  $p$ -polarized probe field gives  $s$ -polarized phase conjugated response. In this case, pump field 1 is  $s$  polarized while pump field 2 is  $p$  polarized ( $spp$ ). The response is plotted as isophotes [ $m^4/W^2$ ] on a logarithmic scale as a function of (i) the frequency  $\omega$  normalized to the transition frequency  $\omega_{12}$  and (ii) the parallel component of the wave vector, normalized to the vacuum wave number. The difference between two neighboring contours is one order of magnitude. The absolute amplitude of the isophote of value  $10^{-20} m^4/W^2$  has been plotted using a long-dashed curve and the isophote with magnitude  $10^{-30} m^4/W^2$  with a short-dashed curve. The strip below is plotted in a linear scale in  $q_{\parallel}/q$  while the rest is on a logarithmic scale.

is  $\Xi_{yyyy}$ . Altogether the phase conjugated response in this purely  $s$ -polarized case (called “ $sss$ ”) is negligible, since it is tens of orders of magnitude less than those of the other combinations. If, on the other hand, the pump fields are  $p$  polarized ( $pps$ ),  $\Xi_{yyzz}$  is the element of the nonlinear conductivity tensor that contributes. Plotted as isophotes (contours of equal intensity) in the normalized  $\omega$ - $q_{\parallel}$  plane ( $\omega$  normalized to the interband transition frequency  $\omega_{21}$  and  $q_{\parallel}$  normalized to the vacuum wave number  $\omega/c_0$ ), the result is shown in Fig. 3.

Two other combinations of polarization give  $p$ -polarized response using a  $p$ -polarized probe field. As above, the pump

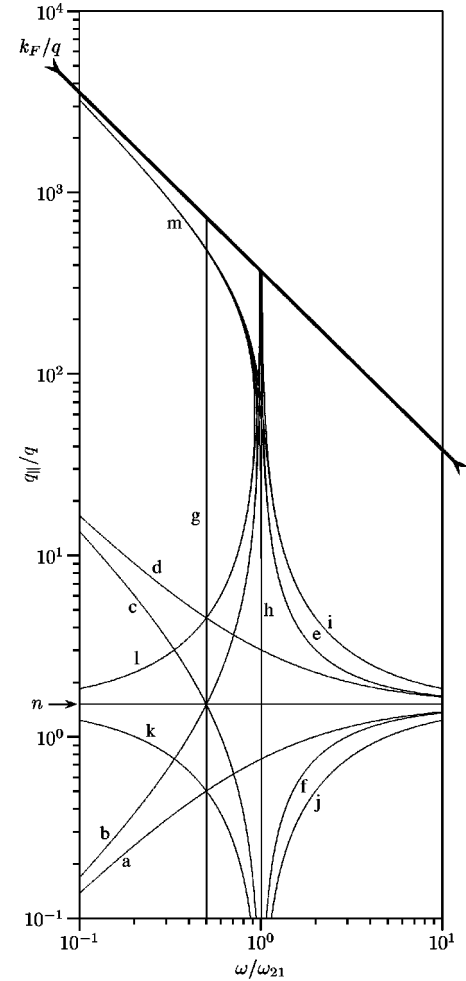


FIG. 7. Resonances of the nonlinear conductivity tensor are shown as a function of (i) the optical frequency normalized to the transition frequency ( $\omega/\omega_{21}$ ) and (ii) the parallel component of the wave vector normalized to the vacuum wave number ( $q_{\parallel}/q$ ). This figure shows only the pure resonances. The broadening due to the relaxation times is neglected by setting them all to infinity.

fields have to be of the same polarization, and can either be  $s$  or  $p$  polarized. With  $s$ -polarized pump fields ( $ssp$ , four tensor elements of the nonlinear conductivity tensor contribute to the phase conjugated response (see Table I). The phase conjugated response is shown in the normalized  $\omega$ - $q_{\parallel}$  plane in Fig. 4. In the other case, another four tensor elements of the nonlinear conductivity tensor contribute to the phase conjugated response when the pump fields are  $p$  polarized (see Table I). We have in Fig. 5 shown the phase conjugated response for this configuration ( $ppp$ ) in the normalized  $\omega$ - $q_{\parallel}$  plane.

In the remaining four cases, the response has a different polarization than the probe field. This is obtainable by the use of differently polarized pump fields. In order to achieve an  $s$ -polarized response from a  $p$ -polarized probe field one makes use of two differently polarized pump fields, and four tensor elements of the DFWM response tensor contribute to the solution, cf. Table I. Similarly, two differently polarized pump fields are needed in order to produce a  $p$ -polarized response from an  $s$ -polarized source. For this process, another four tensor elements of the nonlinear conductivity tensor contributes according to Table I. Since the resonance

structure of these last four cases are similar, it is sufficient here to discuss the result obtained for just one of those cases. Thus, in Fig. 6 the result is shown for the case where pump field 1 is *s* polarized and pump field 2 and the probe are *p* polarized (*spp*).

The IB model only offers a crude description of the electronic properties of a quantum well, since, for example, the electron density profile at the ion-vacuum edge is poorly accounted for. This gives too sharp a profile and underestimates the spill-out of the wave function. Altogether one should be careful to put too much reality into the IB model when treating local-field variations (related to, say,  $q_{\parallel}$  or  $q_{\perp}$ ) on the atomic length scale. Furthermore, neglecting the Bloch character of the wavefunctions accounting for the dynamics in the plane of the well is doubtful in investigations of the local field among the atoms of the quantum well. The crucial quantity in the abovementioned context is the Fermi wave number  $k_F = (2m_e \mathcal{E}_F)^{1/2}/\hbar$ , and in relation of Figs. 3–6, only results for  $q_{\parallel}/q$  ratios less than approximately

$$\frac{k_F}{q} = \lambda \sqrt{\frac{ZN_+d}{2\pi} + \frac{1}{4d^2}}, \quad (29)$$

appears reliable. Thus we have cut off our results at the line  $q_{\parallel}/q = k_F/q$  in the  $\omega/\omega_{21} - q_{\parallel}/q$  plane in Figs. 3–6.

In many theoretical studies of the properties of phase conjugated fields it is assumed that the phase conjugator is ideal.<sup>92–94</sup> By this is meant that the phase conjugation reflection coefficient is independent of the angle of incidence of the (propagating) probe field (and maybe also of the state of polarization). As we concluded for the single-level quantum well,<sup>49</sup> and as we can now see for the two-level quantum well in Figs. 3–6 this assumption is not such a good approximation, at least not for a metallic quantum well system.

### B. Resonant structure of the DFWM reflection coefficient

Looking at Figs. 3–6, a number of resonances occur. They can be accounted for from the analytic solution to Eq. (A1) by looking at the denominators appearing in the analytic decomposition of the products, as given by Eqs. (B2) and (B3) in Appendix B. These resonances are shown on the scale of Figs. 3–6 in Fig. 7. In the analytic solution of the

TABLE II. Restrictions on the valid combinations of quantum numbers for a two-level quantum well in the nonlinear conductivity tensor for the three combinations of polarized light of the pump fields treated in this communication. Pump field 1 is indexed *k*, and pump field 2 is indexed *h* in Eq. (A1).

<i>k</i>	<i>h</i>	$\Xi$ terms 3–4	$\Xi$ terms 5–8	$\Xi$ terms 9–10
<i>s</i>	<i>s</i>	$l = v = m$	$v = n \wedge m = l$	$v = n = l$
<i>s</i>	<i>p</i>	$l = v \wedge m \neq l$	$v = n \wedge m \neq l$	$v = n \wedge l \neq v$
<i>p</i>	<i>p</i>	$m \neq l \wedge l \neq v$	$v \neq n \wedge m \neq l$	$v \neq n \wedge l \neq v$

integrals over  $\kappa_{\parallel}$  shown in Appendix B, the solution to the terms with three multiplied denominators is reduced in Eq. (B3) to the problem of finding a basic solution to the integrals over  $\kappa_{\parallel}$  for each of these denominators multiplied by a  $\kappa_{\parallel}$ -independent factor. The resulting integrals do not contain sharp resonances, but the factors in front of them do, when  $a_i b_j - b_i a_j = 0$ , for  $i, j \in \{1, 2, 3\}$  and  $i \neq j$ . In order to make an analytical treatment of the resonances appearing in the nonlinear conductivity tensor we in the following define a term of the nonlinear conductivity tensor as a product of three denominators in Eq. (A1), and number them 1, 2, ..., 12. However, not all terms gives contributions to the result in a two-level quantum well. The terms that does not give any contributions are the terms with a  $2\omega$  contribution in the denominator, i.e., terms 1–2 and 11–12. When the denominators of the rest of the terms (3–10) are put into the form of Eq. (B1), a total of four different *a*'s and nine different *b*'s appear. They are listed in Appendix C. Since we are looking for the location of the resonances in the system it is reasonable in the following analysis to let the respective relaxation times  $\tau_{nm}$  in Eqs. (C5)–(C13) be infinite.

In terms of the *a*'s and *b*'s listed in Appendix C, we observe that the third term of  $\Xi_{ijkh}$  has resonances at (i)  $a_1 b_{nm}^4 - b_{vl}^2 a_2 = 0$ , (ii)  $a_3 b_{nm}^4 - b_{nl}^6 a_2 = 0$ , and (iii)  $a_3 b_{vl}^2 - b_{nl}^6 a_1 = 0$ . After insertion of the relevant *a*'s and *b*'s, substitution of  $k_{\parallel}$  in favor of  $n\omega/c_0$  (since  $k_{\parallel} = n\omega/c_0$  in our treatment), and a normalization of  $q_{\parallel}$  to  $q$ , i.e.,  $q_{\parallel} = (q_{\parallel}/q)\omega/c_0$ , we may solve the resulting second order equations with respect to  $\omega$  as a function of  $q_{\parallel}/q$ . Then resonance condition (i) gives

$$\omega = \frac{m_e c_0^2}{\hbar n q_{\parallel}/q} \frac{n - q_{\parallel}/q}{n + q_{\parallel}/q} \pm \sqrt{\left(\frac{m_e c_0^2}{\hbar n q_{\parallel}/q} \frac{n - q_{\parallel}/q}{n + q_{\parallel}/q}\right)^2 + \frac{2m_e c_0^2}{\hbar^2 (n + q_{\parallel}/q)} \left[\frac{\varepsilon_v - \varepsilon_l}{n} + \frac{\varepsilon_m - \varepsilon_n}{q_{\parallel}/q}\right]}, \quad (30)$$

resonance condition (ii) becomes

$$\omega = \frac{m_e c_0^2}{\hbar n q_{\parallel}/q} \pm \sqrt{\left(\frac{m_e c_0^2}{\hbar n q_{\parallel}/q}\right)^2 + \frac{2m_e c_0^2}{\hbar^2 n} \left[\frac{\varepsilon_n - \varepsilon_l}{n + q_{\parallel}/q} + \frac{\varepsilon_m - \varepsilon_n}{q_{\parallel}/q}\right]}, \quad (31)$$

and condition (iii) is

$$\omega = -\frac{m_e c_0^2}{\hbar n q_{\parallel}/q} \pm \sqrt{\left(\frac{m_e c_0^2}{\hbar n q_{\parallel}/q}\right)^2 + \frac{2m_e c_0^2}{\hbar^2 q_{\parallel}/q} \left[\frac{\varepsilon_v - \varepsilon_l}{n} + \frac{\varepsilon_l - \varepsilon_n}{n + q_{\parallel}/q}\right]}. \quad (32)$$

In some of the above equations, some of the solutions can be ruled out immediately, since, for example, in Eq. (31) the

TABLE III. Resonances generated by Eqs. (30)–(40) are shown as a function of the valid combinations of quantum numbers ( $n, m, v, l$ ) and the sign appearing in front of the square roots. In each of upper and lower parts of the table, the upper row shows the generating equation and the next four rows show the values of the quantum numbers, which can take the value 1 or 2 in a two-level quantum well. The last four rows show the resonances resulting from use of the quantum numbers in the respective equations for each sign + and –, the first two of these rows being associated with the normal term, and the last two with the interchanged term. A zero in the last four rows refers to  $\omega = 0$ , and the letters  $a$ – $l$  refers to the resonances shown in Fig. 7. An asterisk is used when the value of a quantum number is indifferent, and a dash in the output field appears when the result is outside the shown range in Fig. 7. Since Eq. (33) is a linear solution in  $\omega$  the sign does not apply, and the result is listed under the plus sign for simplicity. It should be noted in Eq. (34), that the combinations of quantum numbers that give rise to the resonances  $b, e, i, h$ , and  $l$  are going into resonance  $m$  after they have reached the line at  $\omega/\omega_{21}=1$ .

	Eq. (30)	Eq. (31)	Eq. (32)	Eq. (33)	Eq. (34)	Eq. (35)
$n$	* 1 1 1 2 2 2	* 1 1 1 2 2 2	* 1 1 1 2 2 2	* * *	* * * 1 1 1 2 2 2	* 1 1 1 2 2 2
$m$	$n$ 1 2 2 1 1 2	$n$ 1 2 2 1 1 2	* * * * * *	* 1 2	$n n n$ 2 2 2 1 1 1	$n$ 1 2 2 1 1 2
$v$	* 1 * 2 * 1 2	* * * * * *	$n$ 1 2 2 1 1 2	$m$ 2 1	* 1 2 1 1 2 1 2 2	$n$ 2 1 2 1 2 1
$l$	$v$ 2 $v$ 1 $v$ 2 1	$n$ 2 1 2 1 2 1	$n$ 2 1 2 1 2 1	* * *	$v$ 2 1 1 2 1 2 1 2	* * * * * *
+	- - $d$ $i$ - - $e$	- - - - - -	0 - $h$ $c$ - $h$ -	0 $g$ -	0 $e$ $a$ $d$ $i$ - $h$ $j$ $f$	- - - - - -
-	0 $a$ - - - $j$ -	0 $b$ - - $c$ $h$ -	- - - - - -	- - - - - -	- - - - - -	0 $a$ $d$ - $h$ $f$ $e$
+	0 - - - $c$ $k$ $b$	0 $e$ - $d$ $f$ $h$ $a$	- - - - - -	0 $g$ -	0 $b$ - - $l$ - $h$ $k$ $c$	0 - - - $h$ $c$ $b$
-	- - - $l$ $c$ - $b$	- - - - - -	0 - $h$ $f$ $d$ $h$ -	- - - - - -	- - - - - -	- - - - - -
	Eq. (36)	Eq. (37)	Eq. (38)	Eq. (39)	Eq. (40)	
$n$	* * * * * *	* * * 1 * 1 2 2	* 1 1 1 2 2 2	* 1 1 1 2 2 2	* * * 1 1 1 2 2 2	
$m$	* 1 1 1 2 2 2	$n n n$ 2 * 2 1 1	$n$ 1 2 2 1 1 2	$n$ 1 2 2 1 1 2	$n n n$ 2 2 2 1 1 1	
$v$	$m$ 1 2 2 1 1 2	* 1 2 1 $n$ 2 1 2	* * * * * *	$n$ 2 1 2 1 2 1	* 1 2 1 1 2 1 2 2	
$l$	$m$ 2 1 2 1 2 1	$v$ 2 1 1 $m$ 1 2 2	$n$ 2 1 2 1 2 1	* * * * * *	$v$ 2 1 1 2 1 2 1 2	
+	- - - - - -	- - - - - -	- - $h$ $c$ - - $b$	- - - - - -	- - $b$ - - $l$ - $h$ $c$	
-	0 $h$ $d$ $e$ $a$ $f$ -	0 $g$ - - 0 - $h$ $g$	0 - $h$ $c$ - - $b$	0 $a$ $d$ - $h$ $f$ $e$	0 - $b$ - - - $k$ $h$ $c$	
+	0 $h$ - $b$ - $c$ -	0 $g$ - - 0 - $h$ $g$	0 $a$ $h$ $f$ - - -	0 - - - $h$ $c$ $b$	0 $a$ - - - - $j$ $h$ $f$	
-	- - - - - -	- - - - - -	- - $h$ - $d$ - $e$	- - - - - -	- - $e$ $d$ - $i$ - $h$ -	

minus in front of the square root gives only rise to negative values of  $\omega$  in the “interchanged term” (when  $k_{\parallel} = -n\omega/c_0$ ).

In the fourth term of  $\Xi_{ijkh}$  we observe that in addition to a resonance of type (ii), resonances appear at (iv)  $a_2 b_{nm}^4 - b_{nv}^3 a_2 = 0$  and (v)  $a_3 b_{nv}^3 - b_{nl} a_2 = 0$ . Again inserting the respective  $a$ 's and  $b$ 's from Appendix C, substituting  $n\omega/c_0$  for  $k_{\parallel}$ , and normalizing  $q_{\parallel}$  to the vacuum wave number, resonance condition (iv) becomes

$$\omega = \frac{1}{2\hbar} (\varepsilon_v - \varepsilon_m), \quad (33)$$

and resonance condition (v) is equivalent to Eq. (31), taking into account the interchanged term. In our configuration, the choice of a two-level quantum well puts some restrictions on

the values of the quantum numbers  $n, m, v$ , and  $l$  in order to get a nonzero result. Comparing Eqs. (A1) and (10) we observe that if pump field one (indexed  $k$ ) is  $s$  polarized then  $l = v$ , while  $l \neq v$  if it is  $p$  polarized. Similarly, if the other pump field (indexed  $h$ ) is  $s$  polarized we get  $m = l$ , while we get  $m \neq l$  if it is  $p$  polarized. These conditions are summarized in Table II, and the contributions from Eqs. (30)–(33) to the resonances in Fig. 7 are shown in Table III for the valid combinations of quantum numbers.

The resonances conditions in the fifth term of  $\Xi_{ijkh}$  are (vi)  $a_1 b_{nm}^4 + b_{lm}^1 a_2 = 0$ , (vii)  $a_4 b_{nm}^4 - b_{vm}^5 a_2 = 0$ , and (viii)  $a_4 b_{lm}^1 + b_{vm}^5 a_1 = 0$ . By insertion of the respective  $a$ 's and  $b$ 's from Appendix C, substitution of  $k_{\parallel}$  by  $n\omega/c_0$ , and normalization of  $q_{\parallel}$  to the vacuum wave number, resonance condition (vi) becomes

$$\omega = -\frac{m_e c_0^2}{\hbar (q_{\parallel}/q)^2} \pm \sqrt{\left(\frac{m_e c_0^2}{\hbar (q_{\parallel}/q)^2}\right)^2 + \frac{2m_e c_0^2 n}{\hbar^2 (n - q_{\parallel}/q) q_{\parallel}/q} \left[ \frac{\varepsilon_n - \varepsilon_m}{q_{\parallel}/q} + \frac{\varepsilon_v - \varepsilon_l}{n} \right]}, \quad (34)$$

condition (vii) gives

$$\omega = \frac{m_e c_0^2}{\hbar n q_{\parallel}/q} \pm \sqrt{\left(\frac{m_e c_0^2}{\hbar n q_{\parallel}/q}\right)^2 + \frac{2m_e c_0^2}{\hbar^2 n} \left[ \frac{\varepsilon_m - \varepsilon_n}{q_{\parallel}/q} + \frac{\varepsilon_m - \varepsilon_v}{n - q_{\parallel}/q} \right]}, \quad (35)$$

and case (viii) becomes

$$\omega = \frac{m_e c_0^2}{\hbar n q_{\parallel}/q} \pm \sqrt{\left(\frac{m_e c_0^2}{\hbar n q_{\parallel}/q}\right)^2 + \frac{2m_e c_0^2}{\hbar^2 q_{\parallel}/q} \left[\frac{\varepsilon_m - \varepsilon_l}{n} + \frac{\varepsilon_v - \varepsilon_m}{n - q_{\parallel}/q}\right]}. \quad (36)$$

The sixth term of  $\Xi_{ijkh}$  has a resonance of the type (vi), and further resonances at (ix)  $a_2 b_{nm}^4 - b_{vl}^7 a_2 = 0$  and (x)  $a_4 b_{vl}^7 - b_{vm}^5 a_2 = 0$ . Insertion of the different  $a$ 's and  $b$ 's,  $k_{\parallel} = n\omega/c_0$ , and normalizing  $q_{\parallel}$  to the vacuum wave number gives (ix) resonances at

$$\omega = \frac{m_e c_0^2}{\hbar n q_{\parallel}/q} \frac{n + q_{\parallel}/q}{n - q_{\parallel}/q} \pm \sqrt{\left(\frac{m_e c_0^2}{\hbar n q_{\parallel}/q} \frac{n + q_{\parallel}/q}{n - q_{\parallel}/q}\right)^2 + \frac{2m_e c_0^2}{\hbar^2 n} \left[\frac{n + q_{\parallel}/q}{n - q_{\parallel}/q} \frac{\varepsilon_n - \varepsilon_m}{q_{\parallel}/q} + \frac{\varepsilon_l - \varepsilon_n}{n - q_{\parallel}/q}\right]}, \quad (38)$$

and case (xii) the resonances are equivalent to Eq. (31). The eighth term of  $\Xi_{ijkh}$  has a resonance of the type given in case (xi), and additional resonances at (xiii)  $a_1 b_{nm}^4 - b_{nv}^8 a_2 = 0$  and (xiv)  $a_3 b_{nv}^8 - b_{nl}^6 a_1 = 0$ . Repeating the procedure from above, we get for case (xiii) the solution

$$\omega = \frac{m_e c_0^2}{\hbar n q_{\parallel}/q} \pm \sqrt{\left(\frac{m_e c_0^2}{\hbar n q_{\parallel}/q}\right)^2 + \frac{2m_e c_0^2}{\hbar^2 (n - q_{\parallel}/q)} \left[\frac{\varepsilon_m - \varepsilon_n}{q_{\parallel}/q} + \frac{\varepsilon_n - \varepsilon_v}{n}\right]}, \quad (39)$$

and in case (xiv) gives resonances equivalent to the result given in Eq. (32). Again, when considering a two-level quantum well in our configuration, some restrictions apply to the quantum numbers. If we again compare Eqs. (A1) and (10) we see that if pump field one (index  $k$ ) is  $s$  polarized, then  $v=n$ , and if it is  $p$  polarized, then  $v \neq n$ . Additionally, if pump field two (index  $h$ ) is  $s$  polarized,  $m=l$ , and if it is  $p$  polarized,  $m \neq l$ . This has the consequences that (i) the quantum numbers  $n$  and  $m$  can be chosen arbitrarily when both pump fields are  $s$  polarized, (ii) when both pump fields are  $p$  polarized we either get  $m=n$  and  $l=v$ , or we get  $m=v$  and

$$\omega = \frac{m_e c_0^2}{\hbar n q_{\parallel}/q} \frac{n + q_{\parallel}/q}{n - q_{\parallel}/q} \pm \sqrt{\left(\frac{m_e c_0^2}{\hbar n q_{\parallel}/q} \frac{n + q_{\parallel}/q}{n - q_{\parallel}/q}\right)^2 + \frac{2m_e c_0^2}{\hbar^2 (n - q_{\parallel}/q)} \left[\frac{\varepsilon_m - \varepsilon_n}{q_{\parallel}/q} + \frac{\varepsilon_l - \varepsilon_v}{n}\right]}, \quad (40)$$

and case (xix) has a solution equivalent to the one given in Eq. (36). As before we find by a comparison of Eqs. (A1) and (10) that some selection rules appear when choosing a two-level quantum well in our configuration, since when pump field one (indexed  $k$ ) is  $s$  polarized we get  $v=n$ , and

$$\omega = \frac{m_e c_0^2}{\hbar n q_{\parallel}/q} \pm \sqrt{\left(\frac{m_e c_0^2}{\hbar n q_{\parallel}/q}\right)^2 + \frac{m_e c_0^2}{\hbar^2 n q_{\parallel}/q} [\varepsilon_m + \varepsilon_v - \varepsilon_n - \varepsilon_l]}, \quad (37)$$

and (x) resonances equivalent to those given in Eq. (35). In the seventh term of  $\Xi_{ijkh}$  there is a resonances of the type of case (ix), and furthermore at (xi)  $a_3 b_{nm}^4 - b_{nl}^6 a_2 = 0$  and (xii)  $a_3 b_{vl}^7 - b_{nl}^6 a_2 = 0$ . As in the previous cases we insert the different  $a$ 's and  $b$ 's found in Appendix C, replace  $k_{\parallel}$  with  $n\omega/c_0$ , and normalize  $q_{\parallel}$  to the the vacuum wave number. Then case (xi) gives resonances at

$l=n$ , (iii) when pump field one is  $s$  polarized and the other one  $p$  polarized we get either  $m=v$  or  $l=v$ , and (iv) in the opposite case we get either  $m=v$  or  $m=n$ . These conditions are summarized in Table II, and the contributions from Eqs. (34)–(39) to the resonances in Fig. 7 are shown in Table III for the valid combinations of quantum numbers. It should be noted that in Eq. (34), the combinations of quantum numbers that give rise to the resonances  $b$ ,  $e$ ,  $i$ ,  $h$ , and  $l$  are going into resonance  $m$  after they have reached the line at  $\omega/\omega_{21}=1$ . None of the other equations contributes to resonance  $m$ .

For the ninth term of  $\Xi_{ijkh}$  the resonances are at (xv)  $a_2 b_{nm}^4 - b_{lm}^3 a_2 = 0$ , (xvi)  $a_4 b_{nm}^4 - b_{vm}^5 a_2 = 0$ , and (xvii)  $a_4 b_{lm}^3 - b_{vm}^5 a_2 = 0$ . After insertion of the relevant  $a$ 's and  $b$ 's from Eqs. (C1)–(C13),  $k_{\parallel} = n\omega/c_0$  and a normalization of  $q_{\parallel}$  to the vacuum wave number, the resulting second order equations can be solved with respect to  $\omega$  as a function of  $q_{\parallel}/q$ . Then case (xv) is equivalent to Eq. (33), and cases (xvi) and (xvii) to Eq. (35). Finally, in the tenth term of  $\Xi_{ijkh}$  a resonance of the type given by case (xvi) occur. Two other resonances are located at (xviii)  $a_1 b_{nm}^4 + b_{vl}^9 a_2 = 0$  and at (xix)  $a_4 b_{vl}^9 + b_{vm}^5 a_1 = 0$ , respectively. Inserting the  $a$ 's and  $b$ 's given in Appendix C and using the same substitution and normalization as above, case (xviii) gives

when it is  $p$  polarized,  $v \neq n$ . Similarly, when pump field two (indexed  $h$ ) is  $s$  polarized we get  $l=v$ , and when it is  $p$  polarized,  $l \neq v$ . Then, if both pump fields are  $s$  polarized we may in a two-level quantum well choose  $m=n$  or  $m \neq n$ . In the case where both pump fields are  $p$  polarized, the result is

identically zero. In the case where pump field one is  $s$  polarized and pump field two is  $p$ -polarized we may choose either  $m=l$  or  $m=v$ , while in the opposite case we may choose either  $m=l$  or  $m=n$ . As before, these conditions are summarized in Table II, and the contributions from Eq. (40) to the resonances in Fig. 7 are shown in Table III for the valid combinations of quantum numbers.

In the linear conductivity tensor [Eq. (4)] resonances occur when  $a_2 b_{nm}^4 - a_2 b_{nm}^{10} = 0$ , where

$$b_{nm}^{10} = \frac{1}{\hbar} (\varepsilon_n - \varepsilon_m) + \frac{\hbar q_{\parallel}^2}{2m_e} - i\tau_{nm}^{-1}. \quad (41)$$

The solutions are  $q_{\parallel} = 0$  or  $\omega = 0$ , independent of the values of  $n$  and  $m$ . Adding this resonance to the ones we found in Eqs. (30)–(40) the resonances appearing in Figs. 3–6 have been identified. Q. E. D.

While most of the resonances described above and shown in Fig. 7 are clearly pronounced in Figs. 3–6, the resonance named  $m$  does not appear so clearly, although in Figs. 5 and 6 the curves indicate that something is present around the position of  $m$ . This resonance is striking by the fact that it approaches the Fermi wave number when the frequency approaches zero. It might also be appropriate here to mention that the resonances named  $a$  and  $b$  have the asymptotic value of  $q_{\parallel} = 1/n$  in the low end of the normalized  $q_{\parallel}-\omega$  spectrum, and that the resonances named  $c$  and  $d$  approaches  $q_{\parallel} = n$  for high values of  $q_{\parallel}/q$  and low values of  $\omega/\omega_{21}$ . The resonance named  $h$  is the interband resonance.

## V. DISCUSSION

To give an impression of the magnitude of the phase conjugated response, we have in Figs. 3–6 highlighted the isophotes with magnitude of  $10^{-20}$  and  $10^{-30} \text{ m}^4/\text{W}^2$  by drawing them with a long-dashed curve and a short-dashed curve, respectively. Their positions in the normalized  $q_{\parallel}-\omega$  plane shows quite clearly that most of the area reachable within a single-mode experiment should produce a phase conjugated response of a magnitude comparable to what one gets from second-harmonic generation (compare Refs. 11–16, 18, 19, 95).

Knowing the positions of the resonances in the normalized  $q_{\parallel}-\omega$  plane, one could of course be tempted to plot the magnitude of the phase conjugated response along paths following each of the resonances (e.g., following the path of resonance  $i$ , and its continuation into  $m$ ) in order to give an improved understanding of the importance of the different resonances. However, since it would be rather difficult in an experiment to follow such a path, and since the exact positions of the resonances probably will be shifted in a practical situation, we have chosen not to do so. We have instead in Figs. 8, 9, and 10 plotted the intensity of the phase conjugated field along linear cuts in the normalized  $\omega-q_{\parallel}$  plane at  $q_{\parallel}/q = 0.4$ ,  $q_{\parallel}/q = 3.0$ , and  $\omega/\omega_{21} = 1.5$ , respectively. Following the curves in Figs. 8–10 along their respective path on Figs. 3–6, the appearance and disappearance of each resonance along the path is easily identified. From Figs. 8–10 it also appears that some of the regions in Figs. 3 and 4 with high density of isophotes are zeros rather than resonances.

One of the resonances are of special interest, namely, the

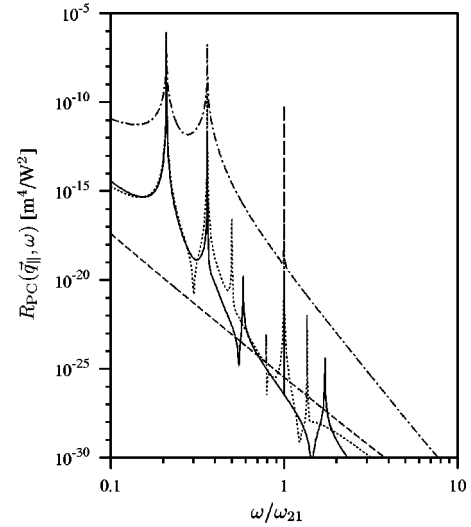


FIG. 8. The phase conjugation reflection coefficient is shown for the four combinations of polarization presented in Figs. 3–6 in the normalized angular frequency range  $0.1 \leq \omega/\omega_{21} \leq 10$  for a constant value of the parallel wave vector,  $q_{\parallel} = 0.4q$ . Thus the four curves represent the *ppp* (dash-dot curve), *pps* (fully drawn curve), *ssp* (dashed curve), and *spp* (dotted curve) configurations.

resonance at the interband transition frequency, which experimentally is rather easy to tune into. Until now, resonant four-wave mixing has been studied in other contexts,<sup>84–87</sup> but always at the point  $(q_{\parallel}, \omega) = (0, \omega_{21})$  in the  $q_{\parallel}-\omega$  plane. To go beyond that, we have plotted the phase conjugated response in the case where the interband transition is resonant (along the linear path in the normalized  $q_{\parallel}-\omega$  plane where  $\omega = \omega_{21}$ ) in Fig. 11.

In configurations with only a single source field in the field-matter interaction, such as, e.g., in linear response, second-harmonic generation, photon drag, and photoemission the so-called self-field approximation has proven to be

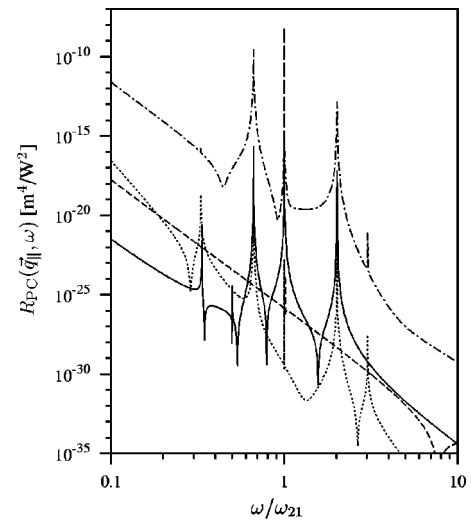


FIG. 9. The phase conjugation reflection coefficient is shown for the four combinations of polarization presented in Figs. 3–6 in the normalized angular frequency range  $0.1 \leq \omega/\omega_{21} \leq 10$  for a constant value of the parallel wave vector  $q_{\parallel} = 3.0q$ . The *ppp* configuration result is drawn using a dash-dot type of curve, while the *pps*, *ssp*, and *spp* configurations are drawn using dotted, dashed, and fully drawn curves, respectively.

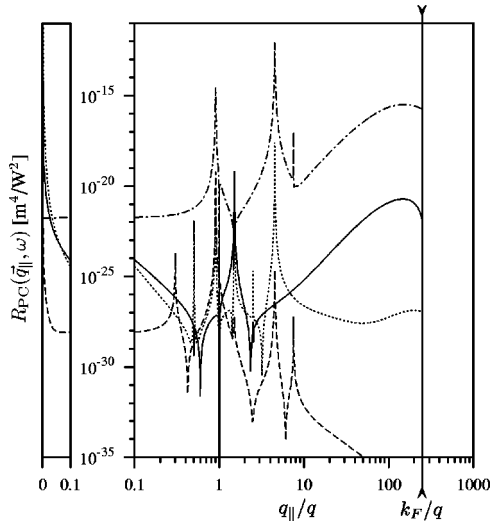


FIG. 10. The phase conjugation reflection coefficient is drawn on a logarithmic scale for the four combinations of polarization presented in Figs. 3–6 in the normalized parallel wave vector range  $0 \leq q_{||}/q \leq k_F/q$  for a constant value of the angular frequency  $\omega = 1.5\omega_{21}$ . In the strip to the left, the abscissa is linear, while it is logarithmic in the right part of the figure. The scale of the ordinate is the same in both frames. The upper curve (dash-dot) shows the result for the *ppp* configuration of polarizations, while the dashed curve shows the *pps* result, the fully drawn curve shows the *ssp* result, and the dotted curve shows the *spp* result.

quite effective. The founding argument to use the self-field approximation is that the dynamics across the quantum well (in the  $z$  direction here) are dominating over motion in the plane of the quantum well ( $x$ - $y$  plane here). Let us as a test in the following look at the consequences of applying the self-field approximation in the present case of degenerate four-wave mixing, where three incident fields are present.

Working within the framework of the self-field approximation, we observe from Eq. (3) that the phase conjugated response would have been limited to the cases where nonlinear and linear current densities is produced in the  $z$  direction. Hence, only tensor elements with  $i=z$  would contribute. Then, from Table I we observe that the contributions from (i) the two cases where the pump fields have the same polarization and the probe field is  $s$  polarized (*sss* and *pps*), and (ii) the mixed-pump configurations *spp* and *psp* would have been neglected. Thus, the data presented in Figs. 3 and 6 would have been absent. While this is certainly a good approximation in the pure  $s$ -polarized case, the argument is not so good in cases with pump or probe dynamics in the  $z$  direction. Using the argument of the dominating  $z$  dynamics, it is striking that the mixed-pump configurations with  $s$ -polarized probe field survives the self-field approximation while the two others do not, because we would expect more dynamics in the  $z$  direction from the latter two. Another interesting conclusion is that with the loss of Fig. 3 we would also lose the resonances named  $j$ ,  $k$ , and  $l$  in Fig. 7. At the same time we would keep the essentially nonresonant *ssp* case. Comparing the raw amplitudes of the different configurations we can see from Figs. 3–6 and 8–10 that in most regions of the  $q_{||}$ - $\omega$  plane, the *ppp* configuration gives a response that is a few orders of magnitude larger than the other configurations, but we also observe that the three other cases have reso-

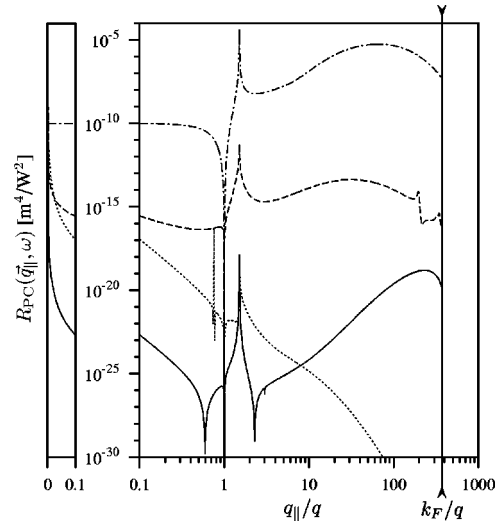


FIG. 11. The phase conjugation reflection coefficient is shown on a logarithmic scale for the four combinations of polarization presented in Figs. 3–6 in the normalized parallel wave vector range  $0 \leq q_{||}/q \leq k_F/q$  when the value of the angular frequency  $\omega = \omega_{21}$ . As in Fig. 10, the strip to the left shows the range  $0 \leq q_{||}/q \leq 0.1$  with linear abscissa, while the rest is plotted with logarithmic abscissa. The scale of the ordinate is the same for both frames. In this figure, the dash-dot curve corresponds to the *ppp* case as in the previous figure, but the dotted curve to the *pps* result. The fully drawn curve corresponds to the *ssp* case as before, and the dashed curve to the *spp* result.

nances around  $q_{||}/q = 0$ , while the *ppp* case do not. Thus, for near-normal incidence of the probe, the phase conjugated reflection coefficient is larger for some of the mixed modes than for the pure  $p$ -polarized configuration, indeed leaving room for experiments that cannot be described within the framework of the self-field approximation.

All in all, we may conclude from the above discussion that although the argument behind the self-field approximation remains intact, when one allows more than one incident field to participate in the interaction (as in, e.g., sum and difference frequency generation, or degenerate four-wave mixing), one should be careful in applying the self-field approximation in cases where mixed polarizations of the incident fields are allowed.

Outside the resonances the influence of the relaxation time is insignificant, but around the resonances the choice of relaxation time has a great influence on the width (in the  $q_{||}$  space) and amplitude of each resonance. Choosing adequate relaxation times  $\tau_{nm}$  is a difficult problem and it appears from Fig. 12 how big impact the relaxation time has on the phase conjugation reflection coefficient. The intraband relaxation time in the occupied state ( $\tau_{11}$ ) has been chosen in accordance with Ref. 49 to be 3 fs. For the unoccupied state the relaxation time  $\tau_{22}$  (see Fig. 2) has been chosen to approach infinity. In the present case where also interband transitions contribute to the phase conjugated response, the intraband relaxation time is of little importance, and thus it is the choice of interband relaxation times (here  $\tau_{21}$  and  $\tau_{12}$ ) that are critical. In the present calculation we assume no relaxation from state  $|1\rangle$  to state  $|2\rangle$ , letting  $\tau_{12} \rightarrow \infty$ .

The phase conjugation reflection coefficient has in Fig. 12

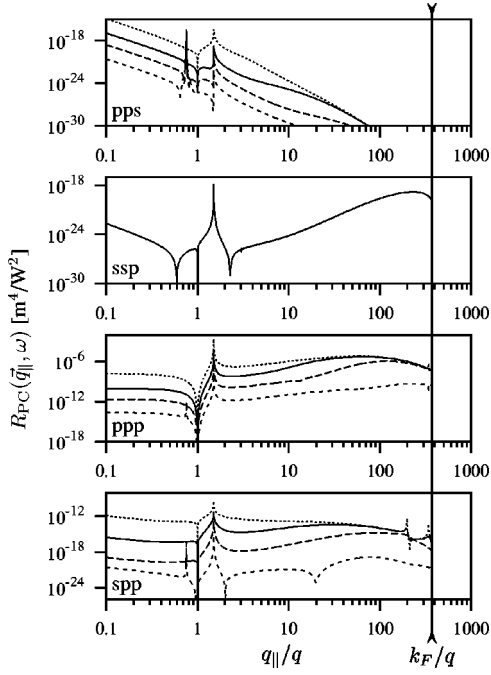


FIG. 12. The phase conjugation reflection coefficient is shown for interband transition resonance for different values of the interband relaxation time  $\tau_{21} \in \{3, 30, 200\}$  fs, and 2 ps. The fully drawn curve corresponds to 200 fs, the long-dashed curve to 30 fs, the short-dashed curve to 3 fs, and the dotted curve to 2 ps.

been plotted for four values of the relaxation time from state  $|2\rangle$  to state  $|1\rangle$ , namely, (i) 30 fs and (ii) 200 fs, which are typical values one would find for bulk copper<sup>91</sup> at (i) room temperature and (ii) at 77 K, (iii) 3 fs, and (iv) 2 ps. The value in case (iii) is obtained by a conjecture based on the difference between measured data for a lead quantum well<sup>96</sup> and the bulk value for lead at room temperature. The difference between the relaxation times measured by Jalochocki, Strózak, and Zdyb<sup>96</sup> is for two monolayers approximately one order of magnitude. Case (iv) is included to see the effect of raising the value of the relaxation time one order of

magnitude, thus essentially assuming a better conductance than in case (ii). The values (i)–(iii) are the same values as we chose in our description of the single-level quantum-well case where only intraband transitions were allowed,<sup>49</sup> but since the interband transition is of a more bulklike character we have in the present calculations chosen  $\tau_{21} = 200$  fs. We notice that in the case where both pump fields are  $s$ -polarized (polarized in the plane of the quantum well), the phase conjugated response does not vary as a function of the interband relaxation time, whereas in the other three cases the general tendency is that they have larger magnitudes for larger values of the relaxation time.

## VI. CONCLUSIONS

Our main conclusion from this work is that DFWM in a thin metallic film gives rise to several resonance structures even in the propagating regime of the  $q_{\parallel}$  spectrum. Furthermore the coupling by the phase conjugation reflection coefficient is of a magnitude that is well within experimental reach. Thus, also single mode excitation in the experimentally feasible regime (up to around  $n=3$ ) should be possible by use of the standard Otto<sup>97</sup> or Kretschmann<sup>98</sup> techniques, and a qualitative comparison with the present work should be possible. However, for a better quantitative comparison in a specific system, it will be necessary to refine the numerical calculation by, e.g., abandoning the IB model in favor of one of the flavors of the KKR, LAPW, or LMTO models, although such a task may prove to be strenuous.

## APPENDIX A: NONLINEAR CONDUCTIVITY TENSOR

Under the assumption that the electron dynamics is free-electron-like in the plane of the quantum well the nonlinear response function  $\tilde{\Xi}(z, z'; \mathbf{q}_{\parallel}, \mathbf{k}_{\parallel}, \omega)$  [given by Eq. (8), and with tensor elements  $\Xi_{ijkh}$ ] can be obtained from the results established for  $\tilde{\Xi}^G(z, z', z'', z'''; \mathbf{q}_{\parallel}, \mathbf{k}_{\parallel}, \omega)$  in Ref. 58. Upon integration over  $z''$  and  $z'''$  [and use of Eq. (9)] one gets

$$\begin{aligned} \Xi_{ijkh}(z, z'; \mathbf{q}_{\parallel}, \mathbf{k}_{\parallel}, \omega) = & -\frac{1}{8\hbar^3} \frac{1}{(2\pi)^2} \frac{2}{(i\omega)^3} \sum_{nmvl} \int \frac{1}{\tilde{\omega}_{nm}(\boldsymbol{\kappa}_{\parallel} + \mathbf{q}_{\parallel}, \boldsymbol{\kappa}_{\parallel}) - \omega} \left\{ \left[ \frac{f_l(\boldsymbol{\kappa}_{\parallel} - \mathbf{k}_{\parallel}) - f_m(\boldsymbol{\kappa}_{\parallel})}{\tilde{\omega}_{lm}(\boldsymbol{\kappa}_{\parallel} - \mathbf{k}_{\parallel}, \boldsymbol{\kappa}_{\parallel}) - \omega} \right. \right. \\ & + \left. \frac{f_l(\boldsymbol{\kappa}_{\parallel} - \mathbf{k}_{\parallel}) - f_v(\boldsymbol{\kappa}_{\parallel})}{\tilde{\omega}_{vl}(\boldsymbol{\kappa}_{\parallel}, \boldsymbol{\kappa}_{\parallel} - \mathbf{k}_{\parallel}) - \omega} \right] \frac{1}{\tilde{\omega}_{vm}(\boldsymbol{\kappa}_{\parallel}, \boldsymbol{\kappa}_{\parallel}) - 2\omega} + \left( \frac{f_l(\boldsymbol{\kappa}_{\parallel} - \mathbf{k}_{\parallel}) - f_v(\boldsymbol{\kappa}_{\parallel})}{\tilde{\omega}_{vl}(\boldsymbol{\kappa}_{\parallel}, \boldsymbol{\kappa}_{\parallel} - \mathbf{k}_{\parallel}) - \omega} + \frac{f_n(\boldsymbol{\kappa}_{\parallel} + \mathbf{q}_{\parallel}) - f_v(\boldsymbol{\kappa}_{\parallel})}{\tilde{\omega}_{nv}(\boldsymbol{\kappa}_{\parallel} + \mathbf{q}_{\parallel}, \boldsymbol{\kappa}_{\parallel}) + \omega} \right) \\ & \times \left. \frac{1}{\tilde{\omega}_{nl}(\boldsymbol{\kappa}_{\parallel} + \mathbf{q}_{\parallel}, \boldsymbol{\kappa}_{\parallel} - \mathbf{k}_{\parallel})} \int j_{h,ml}(z'''; 2\boldsymbol{\kappa}_{\parallel} - \mathbf{k}_{\parallel}) dz''' \int j_{k,lv}(z''; 2\boldsymbol{\kappa}_{\parallel} - \mathbf{k}_{\parallel}) dz'' \int j_{j,vn}(z'; 2\boldsymbol{\kappa}_{\parallel} + \mathbf{q}_{\parallel}) \right. \\ & + \left[ \left( \frac{f_l(\boldsymbol{\kappa}_{\parallel} - \mathbf{k}_{\parallel}) - f_m(\boldsymbol{\kappa}_{\parallel})}{\tilde{\omega}_{lm}(\boldsymbol{\kappa}_{\parallel} - \mathbf{k}_{\parallel}, \boldsymbol{\kappa}_{\parallel}) - \omega} + \frac{f_l(\boldsymbol{\kappa}_{\parallel} - \mathbf{k}_{\parallel}) - f_v(\boldsymbol{\kappa}_{\parallel} - \mathbf{k}_{\parallel} + \mathbf{q}_{\parallel})}{\tilde{\omega}_{vl}(\boldsymbol{\kappa}_{\parallel} - \mathbf{k}_{\parallel} + \mathbf{q}_{\parallel}, \boldsymbol{\kappa}_{\parallel} - \mathbf{k}_{\parallel}) + \omega} \right) \frac{1}{\tilde{\omega}_{vm}(\boldsymbol{\kappa}_{\parallel} - \mathbf{k}_{\parallel} + \mathbf{q}_{\parallel}, \boldsymbol{\kappa}_{\parallel})} \right. \\ & \left. + \left( \frac{f_l(\boldsymbol{\kappa}_{\parallel} - \mathbf{k}_{\parallel}) - f_v(\boldsymbol{\kappa}_{\parallel} - \mathbf{k}_{\parallel} + \mathbf{q}_{\parallel})}{\tilde{\omega}_{vl}(\boldsymbol{\kappa}_{\parallel} - \mathbf{k}_{\parallel} + \mathbf{q}_{\parallel}, \boldsymbol{\kappa}_{\parallel} - \mathbf{k}_{\parallel}) + \omega} + \frac{f_n(\boldsymbol{\kappa}_{\parallel} + \mathbf{q}_{\parallel}) - f_v(\boldsymbol{\kappa}_{\parallel} - \mathbf{k}_{\parallel} + \mathbf{q}_{\parallel})}{\tilde{\omega}_{nv}(\boldsymbol{\kappa}_{\parallel} + \mathbf{q}_{\parallel}, \boldsymbol{\kappa}_{\parallel} - \mathbf{k}_{\parallel} + \mathbf{q}_{\parallel}) - \omega} \right) \frac{1}{\tilde{\omega}_{nl}(\boldsymbol{\kappa}_{\parallel} + \mathbf{q}_{\parallel}, \boldsymbol{\kappa}_{\parallel} - \mathbf{k}_{\parallel})} \right] \end{aligned}$$

$$\begin{aligned}
& \times \int j_{h,ml}(z'''; 2\kappa_{\parallel} - \mathbf{k}_{\parallel}) dz''' \int j_{k,vn}(z''; 2\kappa_{\parallel} - \mathbf{k}_{\parallel} + 2\mathbf{q}_{\parallel}) dz'' j_{j,lv}(z'; 2\kappa_{\parallel} - 2\mathbf{k}_{\parallel} + \mathbf{q}_{\parallel}) \\
& + \left[ \left( \frac{f_l(\kappa_{\parallel} + \mathbf{q}_{\parallel}) - f_m(\kappa_{\parallel})}{\tilde{\omega}_{lm}(\kappa_{\parallel} + \mathbf{q}_{\parallel}, \kappa_{\parallel}) + \omega} + \frac{f_l(\kappa_{\parallel} + \mathbf{q}_{\parallel}) - f_v(\kappa_{\parallel} - \mathbf{k}_{\parallel} + \mathbf{q}_{\parallel})}{\tilde{\omega}_{vl}(\kappa_{\parallel} - \mathbf{k}_{\parallel} + \mathbf{q}_{\parallel}, \kappa_{\parallel} + \mathbf{q}_{\parallel}) - \omega} \right) \frac{1}{\tilde{\omega}_{vm}(\kappa_{\parallel} - \mathbf{k}_{\parallel} + \mathbf{q}_{\parallel}, \kappa_{\parallel})} \right. \\
& + \left. \left( \frac{f_l(\kappa_{\parallel} + \mathbf{q}_{\parallel}) - f_v(\kappa_{\parallel} - \mathbf{k}_{\parallel} + \mathbf{q}_{\parallel})}{\tilde{\omega}_{vl}(\kappa_{\parallel} - \mathbf{k}_{\parallel} + \mathbf{q}_{\parallel}, \kappa_{\parallel} + \mathbf{q}_{\parallel}) - \omega} + \frac{f_n(\kappa_{\parallel} + \mathbf{q}_{\parallel}) - f_v(\kappa_{\parallel} - \mathbf{k}_{\parallel} + \mathbf{q}_{\parallel})}{\tilde{\omega}_{nv}(\kappa_{\parallel} + \mathbf{q}_{\parallel}, \kappa_{\parallel} - \mathbf{k}_{\parallel} + \mathbf{q}_{\parallel}) - \omega} \right) \frac{1}{\tilde{\omega}_{nl}(\kappa_{\parallel} + \mathbf{q}_{\parallel}, \kappa_{\parallel} + \mathbf{q}_{\parallel}) - 2\omega} \right] \\
& \times \int j_{h,lv}(z'''; 2\kappa_{\parallel} - \mathbf{k}_{\parallel} + 2\mathbf{q}_{\parallel}) dz''' \int j_{k,vn}(z''; 2\kappa_{\parallel} - \mathbf{k}_{\parallel} + 2\mathbf{q}_{\parallel}) dz'' j_{j,ml}(z'; 2\kappa_{\parallel} + \mathbf{q}_{\parallel}) \Big\} \\
& \times j_{i,nm}(z; 2\kappa_{\parallel} + \mathbf{q}_{\parallel}) d^2\kappa_{\parallel}. \tag{A1}
\end{aligned}$$

## APPENDIX B: ON THE SOLUTION TO THE INTEGRALS OVER $\kappa_{\parallel}$ IN THE LOW-TEMPERATURE LIMIT

In this appendix we discuss how analytical solutions to the integrals over the electronic wave vector  $\kappa_{\parallel}$ , appearing in the linear and nonlinear conductivity tensor may be obtained, and for simplicity the discussion is limited to cover the low-temperature limit. These integrals can, when scattering takes place in the  $x$ - $z$  plane, be expressed as a sum over terms of the general type

$$\mathcal{F}_{pq}^{\beta}(n, \{a\}, \{b\}, s) = \int_{-\infty}^{\infty} \int_{-\infty}^{\infty} \frac{\kappa_x^p \kappa_y^q f_n(\kappa_{\parallel} + s\mathbf{e}_x)}{\prod_{k=1}^{\beta} [a_k \kappa_x + b_k]} d\kappa_x d\kappa_y, \tag{B1}$$

where  $p, k, \beta$  are nonnegative integers, and  $q$  is an even nonnegative integer. The functions depends on (i) the quantum number  $n$ , which is a positive nonzero integer, (ii) a set of real quantities,  $\{a\} \equiv \{a_1, \dots, a_{\beta}\}$  appearing in front of the integration variable  $\kappa_x$  in the denominator, (iii) a set of complex nonzero quantities,  $\{b\} \equiv \{b_1, \dots, b_{\beta}\}$  appearing also in the denominator, and (iv) the real quantity  $s$  representing the displacement (in the  $x$  direction) of the center of the Fermi-Dirac distribution function from  $(\kappa_x, \kappa_y) = (0, 0)$ . The quantity  $s$  together with each element in the set  $\{a\}$  are in general functions of the parallel components of the probe and pump wave vectors,  $\mathbf{q}_{\parallel}$  and  $\mathbf{k}_{\parallel}$ . Each element in the set  $\{b\}$  is furthermore a function of  $\tau$ , the relaxation time.

The combinations of  $p$  and  $q$  needed in Eq. (B1) in order to solve the integrals over  $\kappa_{\parallel}$  in the nonlinear conductivity tensor are  $(p, q) \in \{(0, 0), (0, 2), (0, 4), (1, 0), (1, 2), (2, 0), (2, 2), (3, 0), (4, 0)\}$ , and  $\beta \in \{1, 2, 3\}$ . However, functions with  $\beta = 2$  and  $\beta = 3$  can be expressed in terms of functions with  $\beta = 1$  in the following way:

$$\begin{aligned}
& \mathcal{F}_{pq}^2(n, a_1, a_2, b_1, b_2, s) \\
& = \frac{a_1 \mathcal{F}_{pq}^1(n, a_1, b_1, s) - a_2 \mathcal{F}_{pq}^1(n, a_2, b_2, s)}{a_1 b_2 - a_2 b_1}, \tag{B2}
\end{aligned}$$

and

$$\begin{aligned}
& \mathcal{F}_{pq}^3(n, a_1, a_2, a_3, b_1, b_2, b_3, s) \\
& = \frac{a_1^2 \mathcal{F}_{pq}^1(n, a_1, b_1, s)}{(a_2 b_1 - b_2 a_1)(a_3 b_1 - b_3 a_1)} \\
& + \frac{a_2^2 \mathcal{F}_{pq}^1(n, a_2, b_2, s)}{(a_2 b_1 - b_2 a_1)(a_3 b_2 - b_3 a_2)} \\
& + \frac{a_3^2 \mathcal{F}_{pq}^1(n, a_3, b_3, s)}{(a_3 b_1 - b_3 a_1)(a_3 b_2 - b_3 a_2)}. \tag{B3}
\end{aligned}$$

Equations (B2) and (B3) are given with the provision that the values of the different  $a_k$  are nonzero,  $k \in \{1, 2\}$  in Eq. (B2) and  $k \in \{1, 2, 3\}$  in Eq. (B3). If any  $a_k$ , for instance,  $a_1$ , becomes zero, we see from Eq. (B1) that the order (in  $\kappa_x$ ) of the denominator becomes smaller by 1. This implies that  $\mathcal{F}_{pq}^2(n, 0, a_2, b_1, b_2, s) = \mathcal{F}_{pq}^1(n, a_2, b_2, s)/b_1$  in Eq. (B2). The similar conclusion for Eq. (B3) is  $\mathcal{F}_{pq}^3(n, 0, a_2, a_3, b_1, b_2, b_3, s) = \mathcal{F}_{pq}^2(n, a_2, a_3, b_2, b_3, s)/b_1$ . Analogous reductions applies for any other  $a_k = 0$ .

In the low-temperature limit the Fermi-Dirac distribution function is zero outside the Fermi sphere and equal to one inside, and it is therefore advantageous to shift  $\kappa_x$  by  $-s$ , and afterwards carry out the integrations in polar  $(r, \theta)$  coordinates. Using  $\kappa_x = r \cos \theta$ ,  $\kappa_y = r \sin \theta$ , and  $d\kappa_x d\kappa_y = r dr d\theta$ , the integrals to be solved are of the type

$$\mathcal{F}_{pq}^1(n, a, b, s) = \int_0^{\alpha(n)} \int_0^{2\pi} \frac{r (r \cos \theta - s)^p (r \sin \theta)^q}{b - as + ar \cos \theta} d\theta dr, \tag{B4}$$

dropping the now superfluous index on  $a$  and  $b$ . The upper limit of the radial integration is  $\alpha(n) = \sqrt{k_F^2 - (\pi n/d)^2}$ ,  $k_F > \pi n/d$ . If  $k_F < \pi n/d$ , the Fermi-Dirac distribution function is zero, and thus the integral vanishes. Physically,  $\alpha(n)$  may be characterized as the two-dimensional Fermi wave number for electrons in subband  $n$ .

Since the following treatment is a formal solution of Eq. (B4), we will also drop the reference to  $n$  for brevity, letting  $\alpha \equiv \alpha(n)$ . To solve Eq. (B4), let us make the substitutions

$$\eta \equiv \frac{b - as}{a\alpha}, \quad r \equiv a\alpha, \tag{B5}$$

and thereby turn Eq. (B4) into

$$\mathcal{F}_{pq}^1(\alpha, \eta, s) = \frac{\alpha^q}{a} \int_0^1 \int_0^{2\pi} \frac{u^{q+1} (\alpha u \cos \theta - s)^p (1 - \cos^2 \theta)^{q/2}}{\eta + u \cos \theta} d\theta du, \quad (\text{B6})$$

i.e., compared to the possible values of  $p$  and  $q$ , an expression where the angular integral is expressed as a sum of terms of the form  $\cos^h \theta$  in the nominator, where  $h \in \{0, 1, 2, 3, 4\}$ . To carry out the angular integrals we put  $t = \exp(i\theta)$  so that the integrals become of the type

$$\int_0^{2\pi} \frac{\cos^h \theta}{\eta + u \cos \theta} d\theta = \frac{1}{2^h i u} \oint \frac{(1+t^2)^h}{t^h (t-t_+)(t-t_-)} dt. \quad (\text{B7})$$

In Eq. (B7), the poles at  $t_{\pm}$  in the  $t$  plane are located at

$$t_{\pm} = -\frac{\eta}{u} \pm \sqrt{\left(\frac{\eta}{u}\right)^2 - 1}, \quad (\text{B8})$$

and the integration runs along the unit circle. Since  $t_+ t_- = 1$ , one of these poles is located inside the unit circle while the other is outside. When  $h > 0$  there is an additional pole of order  $h$  at  $t=0$ . Using the unit circle as contour, residue calculations give the nontrivial solutions

$$\int_0^{2\pi} \frac{1}{\eta + u \cos \theta} d\theta = \frac{2\pi}{\sqrt{\eta^2 - u^2}}, \quad (\text{B9})$$

$$\int_0^{2\pi} \frac{\cos \theta}{\eta + u \cos \theta} d\theta = \frac{2\pi}{u} \left[ 1 - \frac{\eta}{\sqrt{\eta^2 - u^2}} \right], \quad (\text{B10})$$

$$\int_0^{2\pi} \frac{\cos^2 \theta}{\eta + u \cos \theta} d\theta = \frac{2\pi\eta}{u^2} \left[ \frac{\eta}{\sqrt{\eta^2 - u^2}} - 1 \right], \quad (\text{B11})$$

$$\int_0^{2\pi} \frac{\cos^3 \theta}{\eta + u \cos \theta} d\theta = \frac{\pi}{u} + \frac{2\pi\eta^2}{u^3} \left[ 1 - \frac{\eta}{\sqrt{\eta^2 - u^2}} \right], \quad (\text{B12})$$

$$\int_0^{2\pi} \frac{\cos^4 \theta}{\eta + u \cos \theta} d\theta = \frac{2\pi\eta^3}{u^4} \left[ \frac{\eta}{\sqrt{\eta^2 - u^2}} - 1 \right] - \frac{\pi\eta}{u^2}. \quad (\text{B13})$$

To finish the formal solution, (i) insert these results into Eq. (B6), (ii) carry out the elementary radial integrations (see, e.g., Ref. 99, Sec. 2.27), (iii) backsubstitute  $\eta$ , and (iv) check convergence for  $a \rightarrow 0$ . Step (iv) can be carried out by use of a binomial series expansion of the square roots appearing,

and a comparison the the result one gets by setting  $a=0$  already in Eq. (B4). The solution to the integrals appearing in Eqs. (4) and (A1) are then found in a straightforward manner, but since the algebraic expressions are rather long, we will omit presenting them here (they can be found in Ref. 89 together with explicit expressions for the case where  $a = 0$ ).

### APPENDIX C: DENOMINATOR COEFFICIENTS

$$a_1 = \frac{\hbar k_{\parallel}}{m_e}, \quad (\text{C1})$$

$$a_2 = \frac{\hbar q_{\parallel}}{m_e}, \quad (\text{C2})$$

$$a_3 = \frac{\hbar}{m_e} (q_{\parallel} + k_{\parallel}), \quad (\text{C3})$$

$$a_4 = \frac{\hbar}{m_e} (q_{\parallel} - k_{\parallel}), \quad (\text{C4})$$

$$b_{nm}^1 = \frac{1}{\hbar} (\varepsilon_n - \varepsilon_m) + \frac{\hbar k_{\parallel}^2}{2m_e} - \omega - i\tau_{nm}^{-1}, \quad (\text{C5})$$

$$b_{nm}^2 = \frac{1}{\hbar} (\varepsilon_n - \varepsilon_m) - \frac{\hbar k_{\parallel}^2}{2m_e} - \omega - i\tau_{nm}^{-1}, \quad (\text{C6})$$

$$b_{nm}^3 = \frac{1}{\hbar} (\varepsilon_n - \varepsilon_m) + \frac{\hbar q_{\parallel}^2}{2m_e} + \omega - i\tau_{nm}^{-1}, \quad (\text{C7})$$

$$b_{nm}^4 = \frac{1}{\hbar} (\varepsilon_n - \varepsilon_m) + \frac{\hbar q_{\parallel}^2}{2m_e} - \omega - i\tau_{nm}^{-1}, \quad (\text{C8})$$

$$b_{nm}^5 = \frac{1}{\hbar} (\varepsilon_n - \varepsilon_m) + \frac{\hbar}{2m_e} (q_{\parallel} - k_{\parallel})^2 - i\tau_{nm}^{-1}, \quad (\text{C9})$$

$$b_{nm}^6 = \frac{1}{\hbar} (\varepsilon_n - \varepsilon_m) + \frac{\hbar}{2m_e} (q_{\parallel}^2 - k_{\parallel}^2) - i\tau_{nm}^{-1}, \quad (\text{C10})$$

$$b_{nm}^7 = \frac{1}{\hbar} (\varepsilon_n - \varepsilon_m) + \frac{\hbar q_{\parallel}}{2m_e} (q_{\parallel} - 2k_{\parallel}) + \omega - i\tau_{nm}^{-1}, \quad (\text{C11})$$

$$b_{nm}^8 = \frac{1}{\hbar} (\varepsilon_n - \varepsilon_m) + \frac{\hbar k_{\parallel}}{2m_e} (2q_{\parallel} - k_{\parallel}) - \omega - i\tau_{nm}^{-1}, \quad (\text{C12})$$

$$b_{nm}^9 = \frac{1}{\hbar} (\varepsilon_n - \varepsilon_m) + \frac{\hbar k_{\parallel}}{2m_e} (k_{\parallel} - 2q_{\parallel}) - \omega - i\tau_{nm}^{-1}. \quad (\text{C13})$$

\*Present address: Fachbereich Physik, Freie Universität Berlin, Arnimallee 14, D-14195 Berlin; and Max-Planck-Institut für Mikrostrukturphysik, Weinberg 2, D-06120 Halle/Saale, Germany. Electronic address: thor@mpi-halle.mpg.de.

<sup>1</sup>P. A. Franken, A. E. Hill, C. W. Peters, and G. Weinrich, Phys. Rev. Lett. **7**, 118 (1961).

<sup>2</sup>A. Liebsch, *Electronic Excitations at Metal Surfaces* (Plenum, New York, 1997).

<sup>3</sup>P. Guyot-Sionnest and Y. R. Shen, Phys. Rev. B **35**, 4420 (1987).

<sup>4</sup>J. F. McGilp, J. Phys. D **29**, 1812 (1996).

<sup>5</sup>C. Weisbuch and B. Vinter, *Quantum Semiconductor Structures: Fundamentals and Applications* (Academic Press, San Diego,

- 1991).
- <sup>6</sup>V. M. Axt and S. Mukamel, *Rev. Mod. Phys.* **70**, 145 (1998).
- <sup>7</sup>R.-P. Pan, H. D. Wei, and Y. R. Shen, *Phys. Rev. B* **39**, 1229 (1989).
- <sup>8</sup>J. Reif, J. C. Zink, C.-M. Schneider, and J. Kirschner, *Phys. Rev. Lett.* **67**, 2878 (1991).
- <sup>9</sup>T. Rasing, in *Nonlinear Optics in Metals*, edited by K. H. Bennemann (Oxford University Press, Oxford, 1998), pp. 132–218.
- <sup>10</sup>R. Vollmer, in *Nonlinear Optics in Metals*, edited by K. H. Bennemann (Oxford University Press, Oxford, 1998), pp. 42–131.
- <sup>11</sup>J. E. Sipe and G. I. Stegeman, in *Surface Polaritons*, edited by V. M. Agranovich and D. L. Mills (North-Holland, Amsterdam, 1982), pp. 661–701.
- <sup>12</sup>G. L. Richmond, J. M. Robinson, and V. L. Shannon, *Prog. Surf. Sci.* **28**, 1 (1988).
- <sup>13</sup>A. Liebsch and W. L. Schaich, *Phys. Rev. B* **40**, 5401 (1989).
- <sup>14</sup>T. F. Heinz, in *Nonlinear Surface Electromagnetic Phenomena*, edited by H.-E. Ponath and G. I. Stegeman (Elsevier, Amsterdam, 1991), pp. 353–416.
- <sup>15</sup>S. Janz and H. M. van Driel, *Int. J. Nonlinear Opt. Phys.* **2**, 1 (1993).
- <sup>16</sup>G. A. Reider and T. F. Heinz, in *Photonic Probes of Surfaces*, edited by P. Halevi (North-Holland, Amsterdam, 1995), pp. 413–478.
- <sup>17</sup>A. Liebsch, in *Photonic Probes of Surfaces*, edited by P. Halevi (North-Holland, Amsterdam, 1995), pp. 479–532.
- <sup>18</sup>K. Pedersen, in *Studies in Classical and Quantum Nonlinear Phenomena*, edited by O. Keller (Nova Science, New York, 1995), pp. 385–418.
- <sup>19</sup>A. Liu and G. W. Bryant, *Phys. Rev. B* **59**, 2245 (1999).
- <sup>20</sup>R. Bavli and Y. B. Band, *Phys. Rev. A* **43**, 5044 (1991).
- <sup>21</sup>S. Chu, *Rev. Mod. Phys.* **70**, 685 (1998).
- <sup>22</sup>W. D. Phillips, *Rev. Mod. Phys.* **70**, 721 (1998).
- <sup>23</sup>C. N. Cohen-Tannoudji, *Rev. Mod. Phys.* **70**, 707 (1998).
- <sup>24</sup>O. Keller, *Phys. Rev. B* **48**, 4786 (1993).
- <sup>25</sup>F. T. Vasko, *Phys. Rev. B* **53**, 9576 (1996).
- <sup>26</sup>X. Chen and O. Keller, *Phys. Rev. B* **55**, 15 706 (1997).
- <sup>27</sup>O. Keller and G. Wang, *Phys. Rev. B* **56**, 12 327 (1997).
- <sup>28</sup>O. A. Aktsipetrov, A. V. Melnikov, T. V. Murzina, A. A. Mikhlin, and A. N. Rubtsou, *Surf. Sci.* **336**, 225 (1995).
- <sup>29</sup>O. A. Aktsipetrov, A. A. Fedyanin, and M. C. Downer, in *Notions and Perspectives of Nonlinear Optics*, edited by O. Keller (World Scientific, Singapore, 1996), pp. 301–338.
- <sup>30</sup>U. Pustogowa, W. Hübner, and K. H. Bennemann, *Surf. Sci.* **307–309**, A1129 (1994).
- <sup>31</sup>A. Liu and O. Keller, *Phys. Scr.* **52**, 116 (1995).
- <sup>32</sup>T. Rasing and M. G. Goerkamp, *Proc. SPIE* **2801**, 96 (1995).
- <sup>33</sup>T. Rasing, in *Notions and Perspectives of Nonlinear Optics*, edited by O. Keller (World Scientific, Singapore, 1996), pp. 339–369.
- <sup>34</sup>J. P. Dewitz, J. Chen, and W. Hübner, *Phys. Rev. B* **58**, 5093 (1998).
- <sup>35</sup>J. S. Nkoma, *J. Phys.: Condens. Matter* **1**, 9623 (1989).
- <sup>36</sup>E. Z. Mishchenko and L. A. Fal'kovskii, *Zh. Eksp. Teor. Fiz.* **107**, 936 (1995) [*Sov. Phys. JETP* **80**, 531 (1995)].
- <sup>37</sup>F. J. Garcia-Vidal and J. B. Pendry, *Phys. Rev. Lett.* **77**, 1163 (1996).
- <sup>38</sup>R. Haight, *Surf. Sci. Rep.* **21**, 275 (1995).
- <sup>39</sup>T. Fauster and W. Steinmann, in *Photonic Probes of Surfaces*, edited by P. Halevi (North-Holland, Amsterdam, 1995), pp. 347–411.
- <sup>40</sup>A. T. Georges, *Phys. Rev. B* **51**, 13 735 (1995).
- <sup>41</sup>V. M. Shalaev, C. Douketis, T. Hasslett, T. Stuckless, and M. Moskovits, *Phys. Rev. B* **53**, 11 193 (1996).
- <sup>42</sup>Y. S. Tergiman, K. Warda, C. Girardeau-Montaut, and J.-P. Girardeau-Montaut, *Opt. Commun.* **142**, 126 (1997).
- <sup>43</sup>M. Wolf, A. Hotzel, E. Knoesel, and D. Velic, *Phys. Rev. B* **59**, 5926 (1999).
- <sup>44</sup>C. Tomas and O. Keller (unpublished); C. Tomas, *Etude de la Corrélation entre Emission Photoélectrique et Génération d'Harmoniques à partir de Métaux* (Université Claude Bernard-Lyons, Lyon, 1998).
- <sup>45</sup>D. von der Linde, in *Notions and Perspectives of Nonlinear Optics* (Ref. 33), pp. 234–271.
- <sup>46</sup>*Atoms in Intense Laser Fields*, edited by M. Gavrila (Academic Press, Boston, 1992).
- <sup>47</sup>J. P. Dewitz, W. Hübner, and K. H. Bennemann, *Z. Phys. D* **37**, 75 (1996).
- <sup>48</sup>Y. Chang, H. R. Fetterman, I. L. Newberg, and S. K. Panaretos, *Appl. Phys. Lett.* **72**, 745 (1998).
- <sup>49</sup>T. Andersen and O. Keller, *Phys. Rev. B* **57**, 14 793 (1998).
- <sup>50</sup>R.-B. Liu and B.-F. Zhu, *Phys. Rev. B* **59**, 5759 (1999).
- <sup>51</sup>E. V. Goldstein and P. Meystre, *Phys. Rev. A* **59**, 1509 (1999).
- <sup>52</sup>L. Deng, E. W. Hagley, J. Wen, M. Trippenbach, Y. Baud, P. S. Julienne, J. E. Simsarian, K. Helmerson, S. L. Rolston, and W. D. Phillips, *Nature (London)* **398**, 218 (1999).
- <sup>53</sup>*Optical Phase Conjugation*, edited by R. A. Fisher (Academic Press, New York, 1983).
- <sup>54</sup>B. Y. Zel'dovich, N. F. Pilipetsky, and V. V. Shkunov, *Principles of Phase Conjugation* (Springer-Verlag, Berlin, 1985).
- <sup>55</sup>D. M. Pepper, in *Laser Handbook, Volume 4*, edited by M. L. Stitch and M. Bass (North-Holland, Amsterdam, 1985), pp. 333–485.
- <sup>56</sup>J.-I. Sakai, *Phase Conjugate Optics* (McGraw-Hill, New York, 1992).
- <sup>57</sup>*Optical Phase Conjugation*, edited by M. Gower and D. Proch (Springer-Verlag, Berlin, 1994).
- <sup>58</sup>T. Andersen and O. Keller, *Phys. Scr.* **58**, 132 (1998).
- <sup>59</sup>M. Fukui, J. E. Sipe, V. C. Y. So, and G. I. Stegeman, *Solid State Commun.* **27**, 1265 (1978).
- <sup>60</sup>K. Ujihara, *Opt. Commun.* **42**, 1 (1982).
- <sup>61</sup>K. Ujihara, *Opt. Commun.* **43**, 225 (1982).
- <sup>62</sup>B. Y. Zel'dovich, N. F. Pilipetskii, A. N. Sudarkin, and V. V. Shkunov, *Dokl. Akad. Nauk SSSR* **252**, 92 (1980) [*Sov. Phys. Dokl.* **25**, 377 (1980)].
- <sup>63</sup>K. Ujihara, *J. Opt. Soc. Am.* **73**, 610 (1983).
- <sup>64</sup>G. I. Stegeman and C. Karaguleff, *J. Appl. Phys.* **54**, 4853 (1983).
- <sup>65</sup>J. M. Nunzi and D. Ricard, *Appl. Phys. B: Photophys. Laser Chem.* **35**, 209 (1984).
- <sup>66</sup>J. M. Nunzi and D. Ricard, *J. Opt. Soc. Am. B* **1**, 458 (1984).
- <sup>67</sup>A. V. Mamaev *et al.*, *Zh. Eksp. Teor. Fiz.* **86**, 232 (1984) [*Sov. Phys. JETP* **59**, 132 (1984)].
- <sup>68</sup>Y. V. Mukhin, N. F. Pilipetskii, A. N. Sudarkin, and K. N. Ushakov, *Dokl. Akad. Nauk SSSR* **285**, 874 (1985) [*Sov. Phys. Dokl.* **30**, 1041 (1985)].
- <sup>69</sup>G. V. Arutyunyan and G. P. Dzhotyan, *Opt. Spektrosk.* **63**, 575 (1987) [*Opt. Spectrosc.* **63**, 338 (1987)].
- <sup>70</sup>N. F. Pilipetskii, A. N. Sudarkin, and K. N. Ushakov, *Zh. Eksp. Teor. Fiz.* **93**, 118 (1987) [*Sov. Phys. JETP* **66**, 66 (1987)].
- <sup>71</sup>T. Andersen and O. Keller, *Opt. Commun.* **155**, 317 (1998).
- <sup>72</sup>E. Abbe, *Arch. Mikrosk. Anat. Entwicklungsmech.* **9**, 413 (1873).
- <sup>73</sup>Lord Rayleigh, *Philos. Mag.* **42**, 167 (1896).

- <sup>74</sup>S. I. Bozhevolnyi, O. Keller, and I. I. Smolyaninov, *Opt. Lett.* **19**, 1601 (1994).
- <sup>75</sup>P. J. Feibelman, *Phys. Rev. B* **12**, 1319 (1975).
- <sup>76</sup>P. J. Feibelman, *Prog. Surf. Sci.* **12**, 287 (1982).
- <sup>77</sup>N. A. W. Holzwarth, G. E. Matthews, R. B. Dunning, A. R. Tackett, and Y. Zeng, *Phys. Rev. B* **55**, 2005 (1997).
- <sup>78</sup>E. E. Krasovskii, *Phys. Rev. B* **56**, 12 866 (1997).
- <sup>79</sup>J. Koringa, *Physica (Amsterdam)* **13**, 392 (1947).
- <sup>80</sup>W. Kohn and N. Rostoker, *Phys. Rev.* **94**, 1111 (1954).
- <sup>81</sup>D. J. Singh, *Planewaves, Pseudopotentials and the LAPW Method* (Kluwer, Boston, 1994).
- <sup>82</sup>O. K. Andersen, *Phys. Rev. B* **12**, 3060 (1975).
- <sup>83</sup>W. Kohn and L. J. Sham, *Phys. Rev.* **140**, A1122 (1965).
- <sup>84</sup>M. Ducloy and D. Bloch, *Phys. Rev. A* **30**, 3107 (1984).
- <sup>85</sup>E. Pawelec, W. Gawlik, B. Samson, and K. Musiol, *Phys. Rev. A* **54**, 913 (1996).
- <sup>86</sup>R. W. Schirmer, M. Y. Lanzerotti, A. L. Gaeta, and G. S. Agarwal, *Phys. Rev. A* **55**, 3155 (1997).
- <sup>87</sup>W. Chafupczak, W. Gawlik, and J. Zachorowski, *Phys. Rev. A* **49**, 4895 (1994).
- <sup>88</sup>O. Keller, *Phys. Rep.* **268**, 85 (1996).
- <sup>89</sup>T. Andersen, *Theoretical Study of Phase Conjugation in Mesoscopic Interaction Volumes* (Institute of Physics, Aalborg University, Aalborg, 1998).
- <sup>90</sup>O. Keller, *Phys. Status Solidi B* **157**, 459 (1990).
- <sup>91</sup>N. W. Ashcroft and N. D. Mermin, *Solid State Physics* (Holt, Rinehart and Winston, New York, 1976).
- <sup>92</sup>B. H. W. Hendriks and G. Nienhuis, *Phys. Rev. A* **40**, 1892 (1989).
- <sup>93</sup>G. S. Agarwal and S. D. Gupta, *Opt. Commun.* **119**, 591 (1995).
- <sup>94</sup>O. Keller, *J. Nonlinear Opt. Phys. Mater.* **5**, 109 (1996).
- <sup>95</sup>X. Chen and O. Keller, *Phys. Status Solidi B* **203**, 287 (1997).
- <sup>96</sup>M. Jalochowski, M. Stróżak, and R. Zdyb (unpublished).
- <sup>97</sup>A. Otto, *Z. Phys.* **216**, 398 (1968).
- <sup>98</sup>E. Kretschmann and H. Raether, *Z. Naturforsch. A* **23**, 2135 (1968).
- <sup>99</sup>I. S. Gradshteyn and I. M. Ryzhik, *Table of Integrals, Series, and Products* (Academic Press, London, 1994).